

Soliton dynamics in a formamide stack using a Taylor-series expansion for the potential surface.

I. Exact equations of motion; dispersion energy

Wolfgang Förner

*Institut für Physikalische und Theoretische Chemie, Friedrich-Alexander-University Erlangen-Nürnberg,
Egerlandstrasse 3, D-8520 Erlangen, Federal Republic of Germany*

(Received 3 March 1989; revised manuscript received 23 June 1989)

The exact equations of motion for a stacked system are derived and their properties are discussed. Results of numerical simulations of soliton dynamics are presented and compared with the previously published ones using an approximate treatment. Qualitative and quantitative differences are found. The intermolecular dispersion energy is included via London's formula into our model of solitary waves in stacked systems. It is shown that first-neighbor terms are of sufficient accuracy. The explicit London formula is fitted by a sixth-order Taylor series. The qualitative properties of solitary waves are not changed too much upon inclusion of dispersion energy. Quantitative changes in velocity, kinetic energy, and effective mass of the waves are found.

I. INTRODUCTION

The concept of solitons is nowadays widely applied for the explanation of certain properties of chemical and physical systems. For example, dynamics of magnetic materials,^{1,2} rotations around σ bonds in polymers³ or phase changes⁴ have been studied using soliton models. A well-known example is the charge transport in lightly doped polyacetylene where solitons are suggested to be the charge carriers.⁵⁻⁷ Also in biologically active materials such as proteins solitons are believed to serve as carriers of energy.⁸ The model suggested by Davydov⁸ was applied to periodic α helices of proteins.⁹ The aperiodic nature of proteins as well as the effects of physiological temperatures on these solitons have been studied by several authors.¹⁰ However, recently the state vector ansatz used in Refs. 8-10 was criticized.¹¹ Also for the dynamics of the sugar phosphate backbone of deoxyribose nucleic acid (DNA) a soliton model was suggested.¹²

Therefore it seems to be reasonable to invoke for the explanation of the nonlocal influence of carcinogens on DNA in chemical carcinogenesis¹³ also a soliton model as suggested and formulated by Ladik and Čížek.¹⁴ However, before attacking the formidable problem of nucleotide base stacks numerically it seems to be reasonable to study the properties of smaller model systems. For this purpose a stacked arrangement of formamide molecules seems to be appropriate.

Within this model system we have shown the existence of solitary waves numerically using a Hückel-type model Hamiltonian.¹⁵ Recently we have shown that the explicit treatment of the π electrons is not necessary (Ref. 16). However, as already mentioned in Ref. 16 for these studies^{15,16} an approximate version of the equations of motion was applied. Therefore, to develop the mathematical model further we present in this work (paper I) of the series a discussion of the exact equations of motion and a comparison to the approximate version of them. Numer-

ical results are also presented.

Further we study the influence of intermolecular dispersion energy, using London's formula¹⁷ which was previously applied to nucleotide base dimers,^{18,19} to larger nucleotide base stacks,^{20,22} and also to the interaction between selenium helices.²³

Finally in the concluding paper (II) (Ref. 24) the explicit inclusion of electron-electron interactions using a Pariser-Parr-Pople-type model for the π electrons is discussed and compared both with the simpler Hückel-type model¹⁵ and the direct potential fit used in Ref. 16 and in this work.

II. METHOD

Formamide has been chosen as the model because the same kinds of nonhydrogen atoms occur also in cytosine. The geometrical arrangement of the molecules is the same as described in detail in Ref. 16 (see Fig. 1). N planar formamide molecules are arranged with parallel molecular planes along the z axis which is perpendicular to those planes. For each molecule three geometrical degrees of freedom are considered. z_n is the negative difference between the actual position Z_n of the plane on the z axis of the n th molecule and its equilibrium position $-(n-1)Z_0 = Z_n^{(e)}$, where $Z_1^{(e)} = 0$. Z_0 is chosen to be 3.36 Å as in B-DNA. ϑ_n is the angle between the C—H bond and its projection onto the plane perpendicular to the z axis. φ_n is the rotation around the z axis relative to its equilibrium value $\phi_n^{(e)} = -(n-1)\phi_0$, with $\phi_0 = 36^\circ$ as in B-DNA. Thus the position vector \mathbf{r}_{in} of atom i in molecule n is related to the position vector \mathbf{r}_{i0} of atom i in a molecule having an unperturbed geometry ($Z_1^{(e)} = \phi_1^{(e)} = \theta_1^{(e)} = 0$) by

$$\mathbf{r}_{in} = \underline{D}'(\varphi_n, \vartheta_n) \mathbf{r}_{i0} - [(n-1)Z_0 + z_n] \mathbf{e}_z. \quad (1)$$

Here \mathbf{e}_z denotes the unit vector in the z direction and

$$\underline{D}'(\varphi_n, \vartheta_n) = \underline{D}(\varphi_n) \cdot \underline{D}(\vartheta), \quad (2)$$

with

$$\underline{D}(\varphi_n) = \begin{pmatrix} \cos\phi_n & \sin\phi_n & 0 \\ -\sin\phi_n & \cos\phi_n & 0 \\ 0 & 0 & 1 \end{pmatrix}, \quad (3)$$

$$\phi_n = (n-1)\phi_0 + \varphi_n,$$

and

$$\underline{D}(\vartheta_n) = \begin{pmatrix} \cos\vartheta_n & 0 & \sin\vartheta \\ 0 & 1 & 0 \\ -\sin\vartheta_n & 0 & \cos\vartheta_n \end{pmatrix}. \quad (3')$$

The total energy E_t is given as the sum of the kinetic energy T and the potential energy V :

$$E_t = T + V, \quad V = V_{\text{HF}} + V_B + E_D. \quad (4)$$

The Hartree-Fock potential V_{HF} is computed as a sum of pair potentials. Each pair potential is expanded into a Taylor series in Δz , $\Delta\vartheta$, and $\Delta\varphi$ and fitted to the *ab initio* Hartree-Fock (HF) potential surface of the dimer shown in Fig. 1 (see Ref. 16 for details). A more detailed discussion of V and of the backbone potential V_B is given in Appendix A.

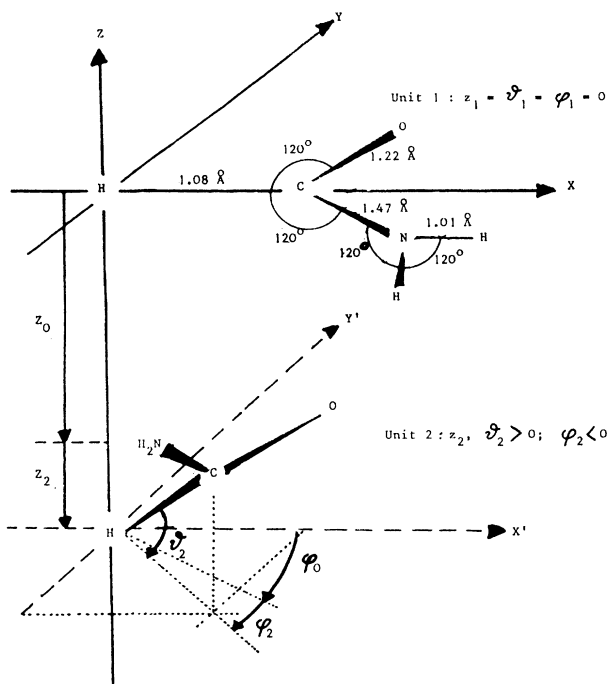


FIG. 1. Geometrical arrangement of a stacked formamide dimer. Molecule 1 is in its equilibrium position and molecule 2 is distorted to $z_2, \vartheta_2, \varphi_2$. Both molecules are planar, molecule 1 is situated in the xy plane, $Z_0 = 3.36 \text{ \AA}$, $\phi_0 = 36^\circ$, and the internal coordinates of the molecules are the same as in Ref. 15.

The dispersion energy E_D is the leading part of the intermolecular correlation energy. In this work we use for the calculation of E_D London's formula¹⁷ which is of empirical origin.

For the intermolecular dispersion energy of an adenine stack -0.2865 eV have been obtained, using the *ab initio* HF method (split valence atomic basis set) and second-order perturbation theory applying the MO's obtained.²⁵ With London's formula and the parameters of Khang and Jhon²⁶ for the corresponding dimer -0.2891 eV was obtained.¹⁹ From this remarkable agreement one can conclude that the use of London's formula for stacked systems seems to be justified.

The dispersion energy E_D^{nm} is given by London's formula as

$$E_D^{nm} = -\frac{3}{2} \sum_g \sum_h \frac{\alpha_g \alpha_h I_g I_h}{I_g + I_h} (R_{gh}^{nm})^{-6}. \quad (5)$$

Here α_g is the atomic polarizability and I_g the valence state ionization potential of atom g . R_{gh}^{nm} is the distance between atom g in molecule n and atom h in molecule m . The details for the calculation of R_{gh}^{nm} from the geometrical degrees of freedom of our model are given in Appendix D. The different α_g and I_g values are taken from Ref. 26 and given in Table I. The total dispersion energy of a stack of N units is calculated to be

$$\begin{aligned} E_D &= 2 \sum_{n=1}^{N-1} \sum_{m=n+1}^N \sum_{g,h} C_{gh} (R_{gh}^{nm})^{-6} \\ &= \sum_{n,m=1}^N (1 - \delta_{n,m}) \sum_{g,h} C_{gh} (R_{gh}^{nm})^{-6}, \end{aligned} \quad (6)$$

with

$$C_{gh} = -\frac{3}{4} \frac{\alpha_g \alpha_h I_g I_h}{I_g + I_h}. \quad (7)$$

For molecular dynamics in addition the derivatives of E_D with respect to z_n , ϑ_n , and φ_n are necessary. Differentiation of (4) with respect to $q_{\mu k}$ ($q_{1k} = z_k$, $q_{2k} = \vartheta_k$, $q_{3k} = \varphi_k$) yields

$$\frac{\partial E_D}{\partial q_{\mu k}} = -12 \sum_{n=1}^N (1 - \delta_{n,k}) \sum_{g,h} C_{gh} (R_{gh}^{nk})^{-7} \frac{\partial R_{gh}^{nk}}{\partial q_{\mu k}}. \quad (8)$$

The differentiation of R_{gh}^{nk} with respect to $q_{\mu k}$ is outlined in Appendix D.

However, as shown numerically in Sec. III second neighbors' dispersion energies turn out to be negligible. Thus in (6) m can be restricted to $n+1$. Furthermore, it

TABLE I. Atomic polarizabilities α and valence state ionization potentials I for the atoms in formamide from Ref. 26.

Atom	α (\AA^3)	I (eV)
C	1.382	11.22
O	0.460	17.25
N	1.090	12.25
H	0.386	13.61

turns out that the dispersion energy can be fitted with a Taylor series in the same way as V_{HF} . Thus finally we can take the *ab initio* Hartree-Fock energies of a dimer in 400 points on the energy hypersurface (in the range $|\Delta z| \leq 0.5 \text{ \AA}$, $|\Delta \vartheta| \leq 15^\circ$, and $|\Delta \varphi| \leq 15^\circ$), the dispersion energies computed by (6), and fit the series (for dimers)

$$(V_{\text{HF}} + E_D) = \sum_{i,j,k \geq 0}^{i+j+k \leq 6} K'_{ijk} \Delta z^i \Delta \vartheta^j \Delta \varphi^k, \quad (9)$$

with the help of a least-squares procedure to the 400 explicitly calculated points as described in detail for V_{HF} alone in Ref. 16. The largest error obtained is 0.24 meV. The shortcomings of this computer-time-saving procedure are discussed in Sec. III. The potential of a stack of N units is then given by

$$(V_{\text{HF}} + E_D) = \sum_{i,j,k \geq 0}^{i+j+k \leq 6} K'_{ijk} \sum_{n=1}^{n-1} \Delta z_n^i \Delta \vartheta_n^j \Delta \varphi_n^k, \quad (10)$$

where $\Delta \mathbf{q}_n = \mathbf{q}_{n+1} - \mathbf{q}_n$.

In Refs. 14–16 the kinetic energy was approximated by

$$T = \sum_{n=1}^N T_n = \frac{1}{2} \sum_{n=1}^N (M \dot{z}_n^2 + \theta_{\vartheta} \dot{\vartheta}_n^2 + \theta_{\varphi} \dot{\varphi}_n^2), \quad (11)$$

where M is the mass of a molecule and the θ 's are the moments of inertia. However, as already pointed out in Ref. 16 the expression is approximative since the three coordinates are not independent. To obtain an exact formula for T one has to use the time derivatives $\dot{\mathbf{r}}_{in}$ of the position vectors \mathbf{r}_{in} of the atoms

$$T_n = \frac{1}{2} \sum_i m_i \dot{\mathbf{r}}_{in}^2, \quad (12)$$

where m_i are the atomic masses. After a rather tedious derivation (see Ref. 16) and using the abbreviation $\mathbf{q}_n^+ = (z_n, \vartheta_n, \varphi_n)$ and the corresponding column vector \mathbf{q}_n one can write

$$T_n = \frac{1}{2} \dot{\mathbf{q}}_n^+ \underline{K}_n \dot{\mathbf{q}}_n, \quad (13)$$

where $[K_n(i, j) = K_n(j, i)]$

$$\begin{aligned} K_n(1, 1) &= M, \\ K_n(2, 1) &= M_z \sin \vartheta_n + M_x \cos \vartheta_n, \\ K_n(3, 1) &= 0, \\ K_n(2, 2) &= M_{xx} + M_{zz}, \\ K_n(3, 2) &= M_{yz} \cos \vartheta_n - M_{xy} \sin \vartheta_n, \\ K_n(3, 3) &= M_{xx} \cos^2 \vartheta_n + M_{yy} + M_{zz} \sin^2 \vartheta_n \\ &\quad + 2 M_{xz} \sin \vartheta_n \cos \vartheta_n. \end{aligned} \quad (14)$$

In (14) the abbreviations

$$M = \sum_i m_i, \quad M_\mu = \sum_i m_i \mu_{i0}, \quad M_{\mu\nu} = \sum_i m_i \mu_{i0} \nu_{i0}, \quad (15)$$

with $\mu, \nu \equiv x, y, z$ have been used. Obviously $K_n(2, 1)$ represents the coupling between ϑ and z . $K_n(2, 2)$ is nothing else than the moment of inertia θ_{ϑ} , while $K_n(3, 3)$

is the moment of inertia θ_{φ} which in the exact treatment is a function of ϑ_n . Therefore also the coupling term $K_n(3, 2)$ between ϑ_n and φ_n appears. However, z_n and φ_n are independent and thus decoupled [$K_n(3, 1) = 0$]. Note that Eqs. (8) and (9) generally are valid, while for the special case treated here $M_z = M_{xz} = M_{yz} = M_{zz} = 0$. On the basis of Eq. (13) one can write down the Hamiltonian function which is useful for quantization as

$$H = T + V = \frac{1}{2} \sum_n \dot{\mathbf{q}}_n^+ \underline{K}_n \dot{\mathbf{q}}_n + V. \quad (16)$$

The exact equations of motion can be obtained using the Lagrange equations of the second type

$$\frac{d}{dt} \frac{\partial L}{\partial \dot{\mathbf{q}}_n} - \frac{\partial L}{\partial \mathbf{q}_n} = 0 \quad (L = T - V) \quad (17)$$

or

$$\frac{d}{dt} \frac{\partial T_n}{\partial \dot{\mathbf{q}}_n} - \frac{\partial T_n}{\partial \mathbf{q}_n} = - \frac{\partial V}{\partial \mathbf{q}_n}. \quad (18)$$

The first term on the left-hand side of (18) leads to

$$\begin{aligned} \frac{d}{dt} \frac{\partial T_n}{\partial \dot{\mathbf{q}}_n} &= \frac{d}{dt} (\underline{K}_n \dot{\mathbf{q}}_n) \\ &= \underline{K}_n \ddot{\mathbf{q}}_n + \dot{\vartheta}_n \frac{\partial \underline{K}_n}{\partial \vartheta_n} \dot{\mathbf{q}}_n \end{aligned} \quad (19)$$

since K_n depends on time only implicitly via ϑ_n . Further,

$$\begin{aligned} \frac{\partial T_n}{\partial \mathbf{q}_n} &= \frac{1}{2} \dot{\mathbf{q}}_n^+ \frac{\partial \underline{K}_n}{\partial \mathbf{q}_n} \dot{\mathbf{q}}_n \\ &= \frac{1}{2} \left[\dot{\mathbf{q}}_n^+ \frac{\partial \underline{K}_n}{\partial \vartheta_n} \dot{\mathbf{q}}_n \right] \mathbf{e}_{\vartheta}, \end{aligned} \quad (20)$$

where $\mathbf{e}_{\vartheta}^+ = (0, 1, 0)$. Thus we obtain

$$\underline{K}_n \ddot{\mathbf{q}}_n + \dot{\vartheta}_n \frac{\partial \underline{K}_n}{\partial \vartheta_n} \dot{\mathbf{q}}_n + \frac{1}{2} \mathbf{e}_{\vartheta} \left[\dot{\mathbf{q}}_n^+ \frac{\partial \underline{K}_n}{\partial \vartheta_n} \dot{\mathbf{q}}_n \right] = - \frac{\partial V}{\partial \mathbf{q}_n}, \quad (21)$$

or in a more compact form

$$\underline{K}_n \ddot{\mathbf{q}} + \mathbf{Q}_n = \mathbf{F}_n, \quad (22)$$

where

$$\mathbf{F}_n = - \frac{\partial V}{\partial \mathbf{q}_n} \quad (23)$$

and

$$\begin{aligned} \mathbf{Q}_n(1) &= (M_z \cos \vartheta_n - M_x \sin \vartheta_n) \dot{\vartheta}_n^2, \\ \mathbf{Q}_n(2) &= Y_n \dot{\varphi}_n^2, \end{aligned} \quad (24)$$

$$\mathbf{Q}_n(3) = -(M_{xy} \cos \vartheta_n + M_{yz} \sin \vartheta_n) \dot{\vartheta}_n^2 - 2 Y_n \dot{\vartheta}_n \dot{\varphi}_n,$$

with

$$Y_n = (1 - 2 \cos^2 \vartheta_n) M_{xz} + (M_{xx} - M_{zz}) \sin \vartheta_n \cos \vartheta_n. \quad (25)$$

The relation of these exact equations of motion to the approximate ones of Refs. 14–16 is discussed Appendix

B, while in Appendix C some constants of motion are derived. These are total energy E_t , the z component of the total momentum P_z , and z component of the total angular momentum L_z .

For the solution of Eqs. (22) one can rewrite them as

$$\ddot{\mathbf{q}}_n = \underline{K}_n^{-1}(\mathbf{F}_n - \mathbf{Q}_n) \quad (26)$$

since it can be numerically verified that for our model system $\underline{K}_n(\vartheta_n)$ is nonsingular in the full range of ϑ_n . Equation (21) can be solved numerically using a Runge-Kutta algorithm correct up to fourth order in the time step.²⁷ A time step size of $\tau=0.005$ ps proved to be sufficient to keep the total energy constant within $\approx 0.1\%$ of the time average of the total kinetic energy.

III. RESULTS AND DISCUSSION

A. Equations of motion and backbone potential

Here we want to study the effects of the additional backbone potential $V_B^{(2)}$ (see Appendix A) as well as of the exact equations of motion in comparison of the approximate equations. For this purpose the dispersion term E_D has not been included in the calculations reported in Sec. III A. We have used a stack of 50 formamide units for this purpose where the first and last molecule has been kept fixed. In this way the somewhat artificial linear potential terms $V_B^{(1)}$ (see Appendix A) can be avoided. As initial excitation $z_2 = -0.4$ Å and $z_{49} = 0.3$ Å is used. In this way the collision of two solitary waves can be studied and due to their different kinetic energies one can also decide if reflection or penetration occurs upon collision.

In Fig. 2 we show the local kinetic energy T_n as a function of site index n and of time t , for the different cases studied. These are applications of the approximate equations of motion without [Fig. 2(a)] and with [Fig. 2(b)] backbone potential $V_B^{(2)}$, and application of the exact equations of motion for the same two cases [Figs. 2(c) and 2(d)]. In Fig. 2(a) one observes, as expected from the results of Ref. 16, two narrow solitary waves which carry different kinetic energies, but having the same velocities. They cross each other without any visible perturbation. As Fig. 2(b) shows there are no longer solitons present in the system (approximate equations of motion) if the backbone potential $V_B^{(2)}$ is applied. The main difference between the systems corresponding to Figs. 2(a) and 2(b) is that in the former case the total potential is only a function of $\Delta\mathbf{q}_n$ while in the latter it depends also on the individual ϑ_n coordinates. This agrees with preliminary calculations on double helices where due to the hydrogen-bonds potential terms of this kind also appear. In these calculations using the approximate equations of motion also no solitary waves could be found.²⁸

If the exact equations of motion are applied the situations is reversed. Without $V_B^{(2)}$ no solitary waves occur [Fig. 2(c)], while with $V_B^{(2)}$ there are solitary waves in the system [Fig. 2(d)]. However, in contrast to the approximate equations of motion their velocity is now dependent on the kinetic energy carried away. The soliton velocities

are somewhat smaller than in the case of the approximate equations, the kinetic energies carried larger. Thus the kinetic masses of the solitons are considerably larger if the exact equations are applied.

Therefore in case of realistic systems like DNA, where

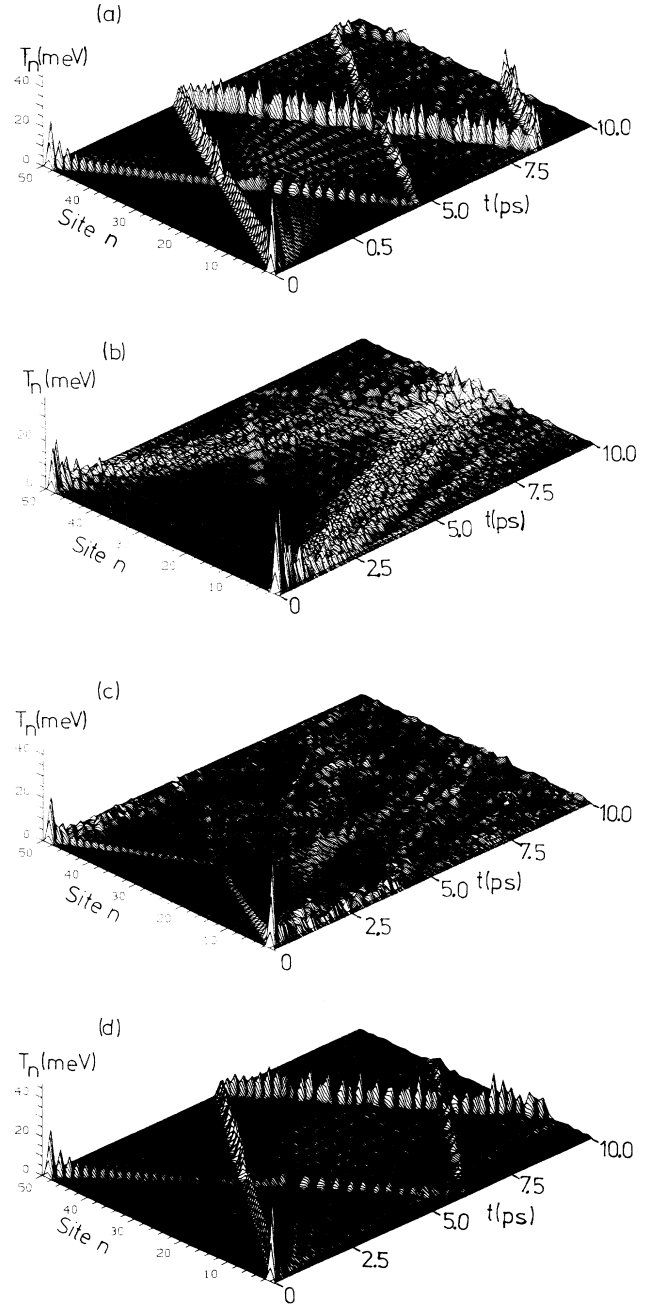


FIG. 2. The local kinetic energy T_n of a stack of 50 formamide units as function of site n and time t using fixed chain ends and an initial excitation of $z_2 = -0.4$ Å and $z_{49} = +0.3$ Å. (a) Approximate equations of motion, $V_B^{(2)}=0$. (b) Approximate equations of motion, $V_B^{(2)}\neq 0$. (c) Exact equations of motion, $V_B^{(2)}=0$. (d) Exact equations of motion, $V_B^{(2)}\neq 0$.

due to the backbone and to the hydrogen bonds certainly potential terms depending on q_n instead of only Δq_n occur, the use of the exact equations of motion is of utmost importance. First of all, the approximate equations would artificially predict the absence of solitary waves in the system, secondly the properties of the waves occurring in both systems of equations, are rather different.

The absence of solitary waves in absence of $V_B^{(2)}$ for the exact equations of motion has to be discussed in some more detail. For this purpose we used an initial excitation of $z_1 = -0.5 \text{ \AA}$ and an open chain of 50 units. The effects we would like to discuss occur also in the system shown in Fig. 2(c) but are more obvious in the system shown in Fig. 3. In Fig. 3(a) the local kinetic energy is shown again. Obviously the excitation emits shock waves without solitary character. Figure 3(b) shows total and total kinetic energy. $T(t)$ is an oscillatory function with no special features. To obtain a deeper insight into the problem we use in Fig. 3(c) the same presentation of the time evolution as in Ref. 16. The ordinate shows the time

in picoseconds. For each time step displayed a dashed line represents the stack axis. The abscissa shows z in bohrs and z_n in bohrs/6. For a better visualization the deviations z_n , ϑ_n , and φ_n from equilibrium were multiplied by 6. Thus each molecule is shown at the position $(n-1)Z_0 + 6z_n$ and is symbolized by a triangle. The rotation axis for the ϑ_n are displayed as being perpendicular to the paper plane for all molecules. Therefore $6\vartheta_n$ is shown directly as the rotation of the triangle. Finally, $6\varphi_n$ is given by the base line of the triangle symbolizing molecule n . If φ_n is positive the triangle stands on its base line; if φ_n is negative it stands on its top corner. Obviously in this case the whole stack is moved along the z axis accompanied by a large rotation of the units both in ϑ_n and φ_n . Since the potential is only a function of Δq_n , simultaneous shifts of all coordinates can occur isoenergetically. While in the approximate equations of motion such motions are forbidden by the conservation laws this is not the case in the exact equations. Here a simultane-

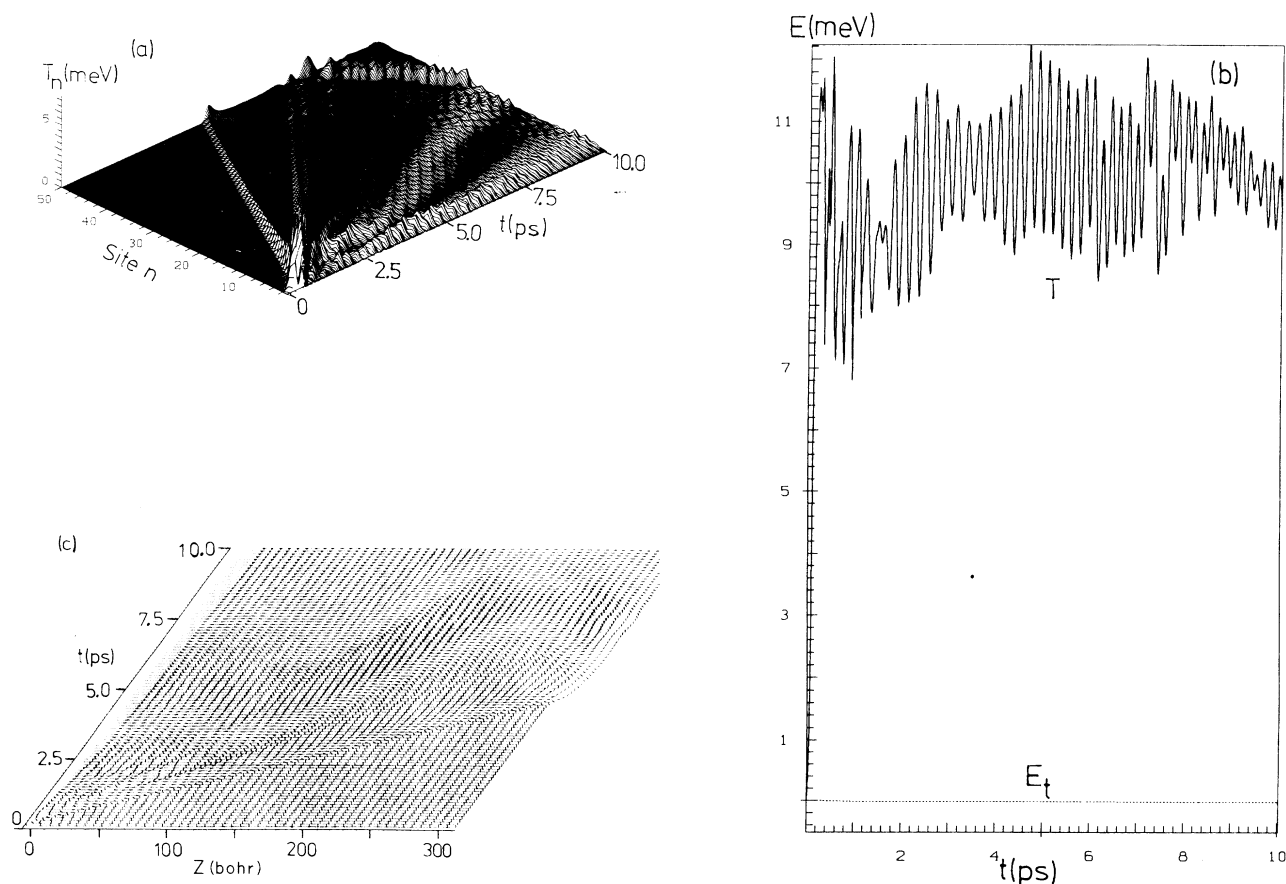


FIG. 3. Time evolution of a stack of 50 formamide units using open ends after an initial excitation of $z_1 = -0.5 \text{ \AA}$ applying the exact equations of motion and $V_B^{(2)}=0$. (a) Local kinetic energy T_n as function of site n and time t . (b) Total energy E_t , relative to its initial value (dotted line) and total kinetic energy T (solid line) as functions of time (t). (c) Time evolution of the coordinates as described in the text.

ous shift of all z_n must be accompanied by a similar shift of all ϑ_n to conserve the component of momentum P_z (see Appendix C). Consequently a similar shift of all φ_n must occur to conserve the angular momentum component L_z . At the end of simulation all z_n values are between 1.3 and 1.7 Å, all ϑ_n values between -75° and -87° , and the φ_n values between -26° and 12° . Thus the system in this case relaxes to an unrealistic geometry which has rather low energy and can be reached by a momentum and angular momentum conserving motion. (The two momenta are conserved to 0.5×10^{-4} and 0.6×10^{-3} a.u., respectively; a.u. = atomic units.) The introduction of $V_B^{(2)}$ which depends on ϑ_n instead of $\Delta\vartheta_n$ makes this relaxation energetically unfavorable and the initial excitation relaxes by emitting a solitary wave whose motion also conserves P_z and L_z .

Finally, one has to explain the reasons why use of the backbone potential $V_B^{(2)}$ together with the approximate equations of motion does not lead to soliton formation. In Figs. 4(a) and 4(b) we compare the approximate (without $V_B^{(2)}$) and exact (with $V_B^{(2)}$) equations of motion for a stack of 30 units. From Figs 4(a) and 4(b) one can see that there are no qualitative differences between the two solitary waves. Only its velocity is reduced if the exact equations are used. In Figs. 5(a) and 5(b) the coordinates z_n , ϑ_n , and φ_n are plotted as a function of site n for different time steps. Obviously the soliton formed in the approximate model has a complex structure with maxima in z_n (≈ 0.3 Å), ϑ_n ($\approx 8^\circ$), and in φ_n ($\approx 1^\circ$) traveling together. At 3 ps the wave is already reflected. If $V_B^{(2)}$ is included a much larger energy is needed to obtain ϑ values up to $\approx 8^\circ$. Since the solitary wave (using the ap-

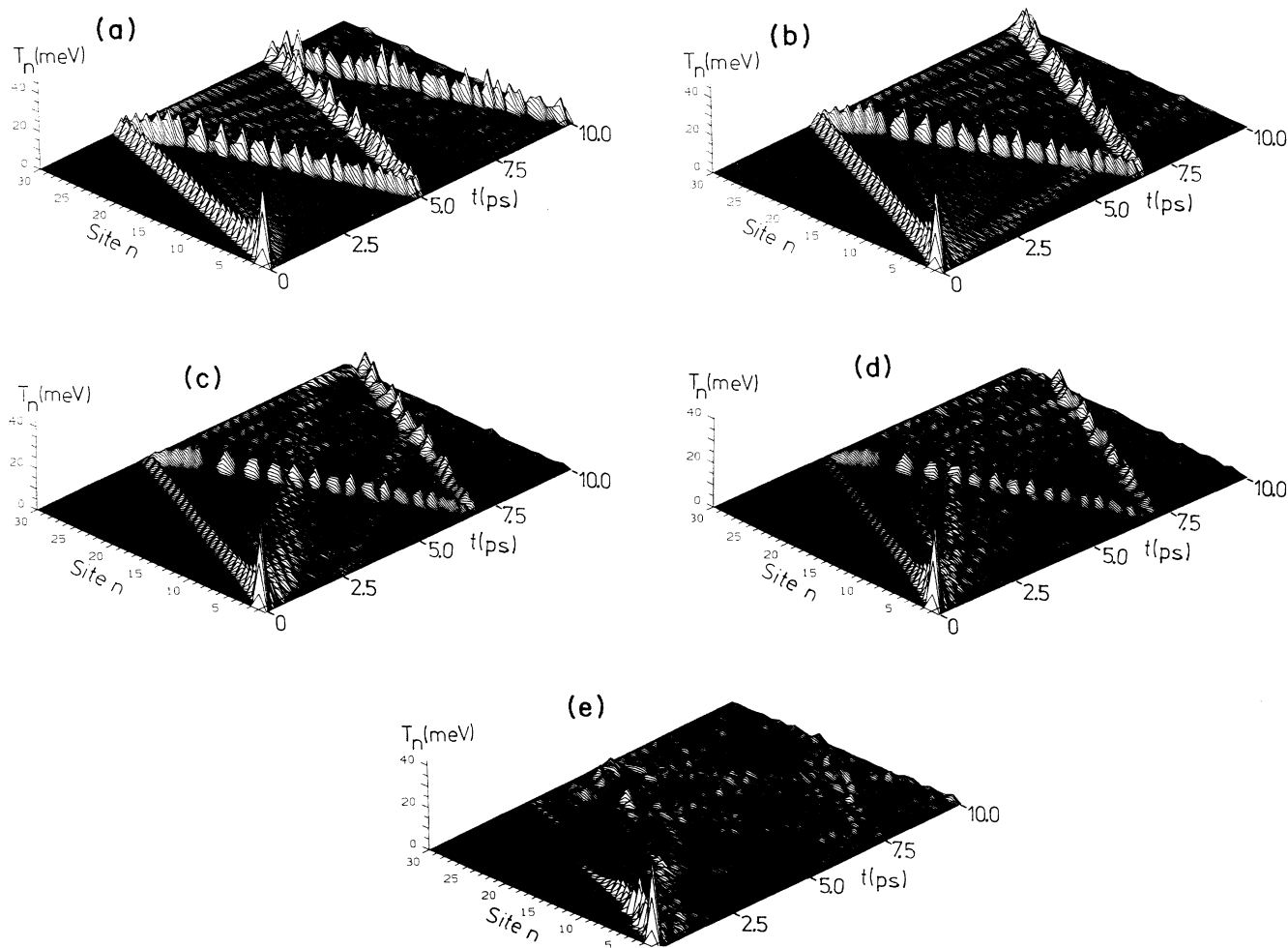


FIG. 4. Comparison of the effect of the strength of the backbone potential using $V_B^{(2)}=0$ together with approximate equations of motion (a) and $V_B^{(2)}$ (b), $0.1V_B^{(2)}$ (c), $0.05V_B^{(2)}$ (d), and $0.01V_B^{(2)}$ (e) together with exact equations of motion for a system of 30 units and fixed chain ends after an initial excitation of $z_2 = -0.4$ Å. Time evolution of the local kinetic energy (T_n) as function of site and time.

proximate equations) has a composite structure in all variables it cannot form in the low-energy region if $V_B^{(2)}$ is included. As seen also from Fig. 6(b) the exact equations allow also solitons which are formed only from structures in the z and φ coordinates.

As mentioned in Appendix A, the backbone potential $V_B^{(2)}$ may have been constructed from a too rigid model compared to realistic systems like DNA where the backbone is more flexible. To estimate how strong $V_B^{(2)}$ has to be at least to allow soliton formation (using the exact equations) we have performed simulations using $0.1V_B^{(2)}$, $0.05V_B^{(2)}$, and $0.01V_B^{(2)}$ as backbone potential. The results are shown in Figs. 4(c), 4(d), and 4(e). Obviously one can reduce $V_B^{(2)}$ to $\frac{1}{20}$ of its magnitude and still observe a soliton. Only for $\frac{1}{100}V_B^{(2)}$ the soliton cannot be formed because the energy barrier is then small enough that again the unphysical state discussed above can be reached. The form of the soliton does not change too much upon reduction of $V_B^{(2)}$ until $0.05V_B^{(2)}$. Only oscillations in the ϑ coordinates start to occur. In Table II the soliton properties obtained from the five calculations shown in Figs 6 and 7 are summarized. As already discussed the main differences between approximate and exact equa-

TABLE II. Time t_0 a solitary wave needs to travel once through a stack of 30 units (fixed chain ends, 90.72 Å) after an initial excitation of $z_2 = -0.4$ Å (excitation energy $V^{(0)} = 50.32$ meV), mean value \bar{T} of kinetic energy, velocity v_s of the wave, and its kinetic mass m^* (in electron masses $m_e, m^* = 2\bar{T}/v_s^2$) using approximate (A) and exact (E) equations of motion and different strengths of the backbone potential V_B ($V_B = \alpha V_B^{(2)}$).

Method	α	t_0 (ps)	\bar{T} (meV)	v_s (km/s)	m^* (m_e)
A	0.00	2.5	26.69	3.63	710
E	1.00	3.3	27.68	2.75	1290
E	0.10	3.5	26.32	2.59	1380
E	0.05	3.6	25.75	2.52	1430
E	0.01	no solitary wave present			

tions of motion are reduction of soliton velocity by $\approx 36\%$ and an increase of kinetic mass by $\approx 82\%$. Reduction of $V_B^{(2)}$ reduces the kinetic energy carried and the velocity, but increases the kinetic mass. From these results one can conclude that the actual strength of the

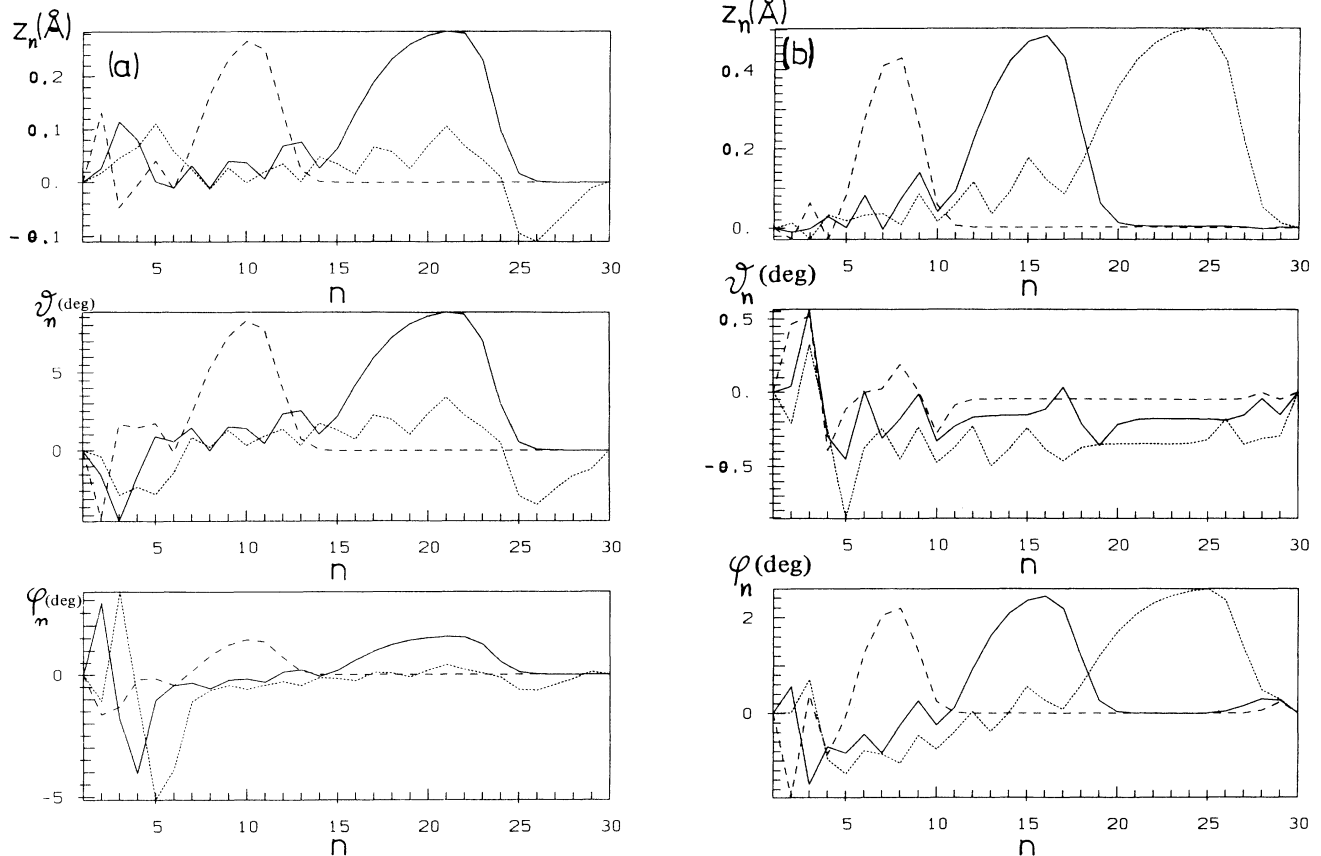


FIG. 5. Same as Figs. 4(a) and 4(b), but showing the coordinates z_n , ϑ_n , and φ_n as functions of site n at time $t = 1$ ps (---), 2 ps (—), and 3 ps (⋯).

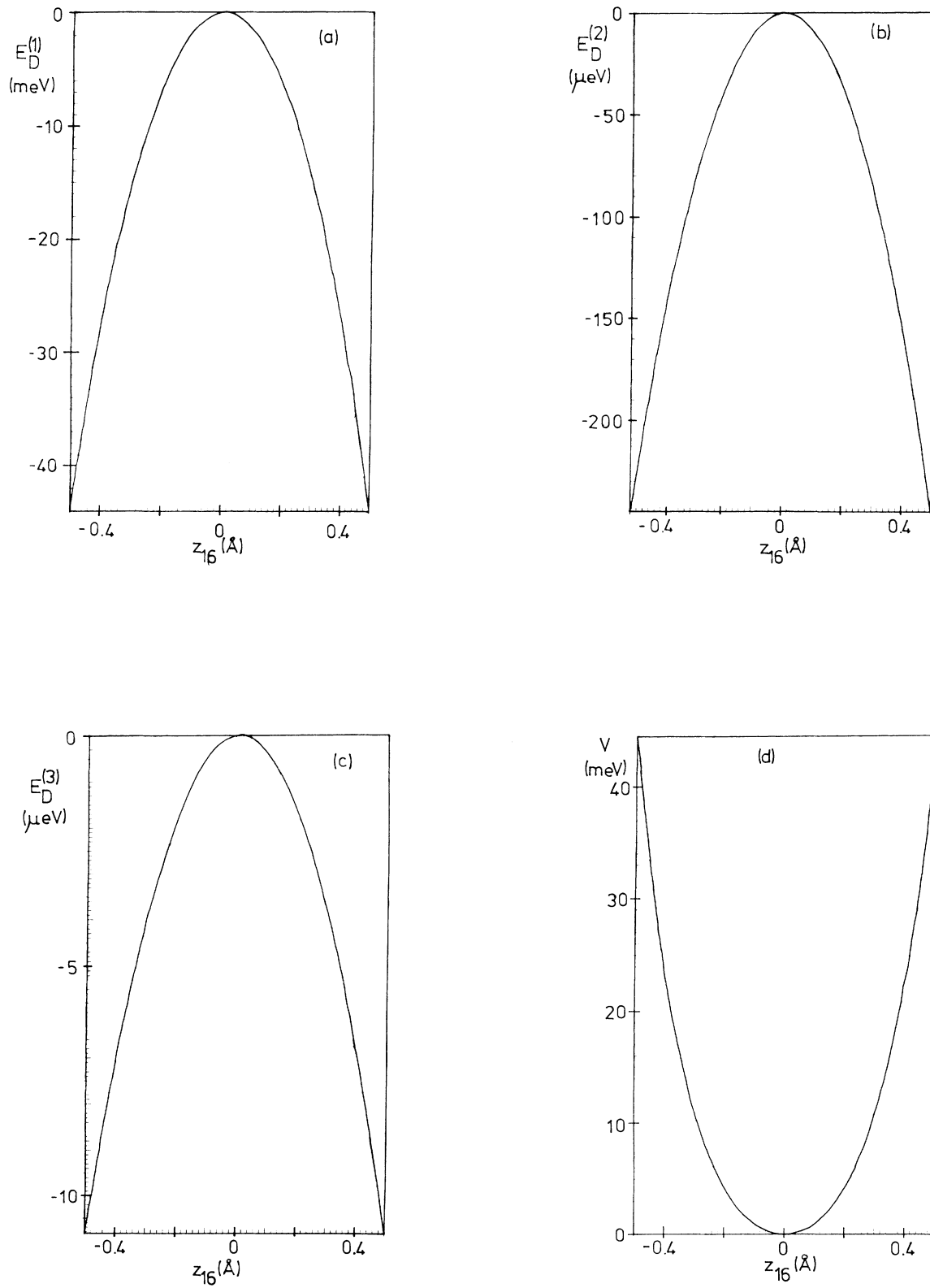


FIG. 6. Dispersion energy terms $E_D^{(n)}$ [$n = 1$ (a), $n = 2$ (b), and $n = 3$ (c)] in a stack of 31 units as function of the central z coordinate (z_{16}), the potential ($V_{HF} + E_D^{(1)}$) as function of the central coordinates z_{16} (d), ϑ_{16} (e), and φ_{16} (f), and the total potential ($V_{HF} + E_D^{(1)} + V_B^{(1)}$) as function of the first z coordinate z_1 (g).

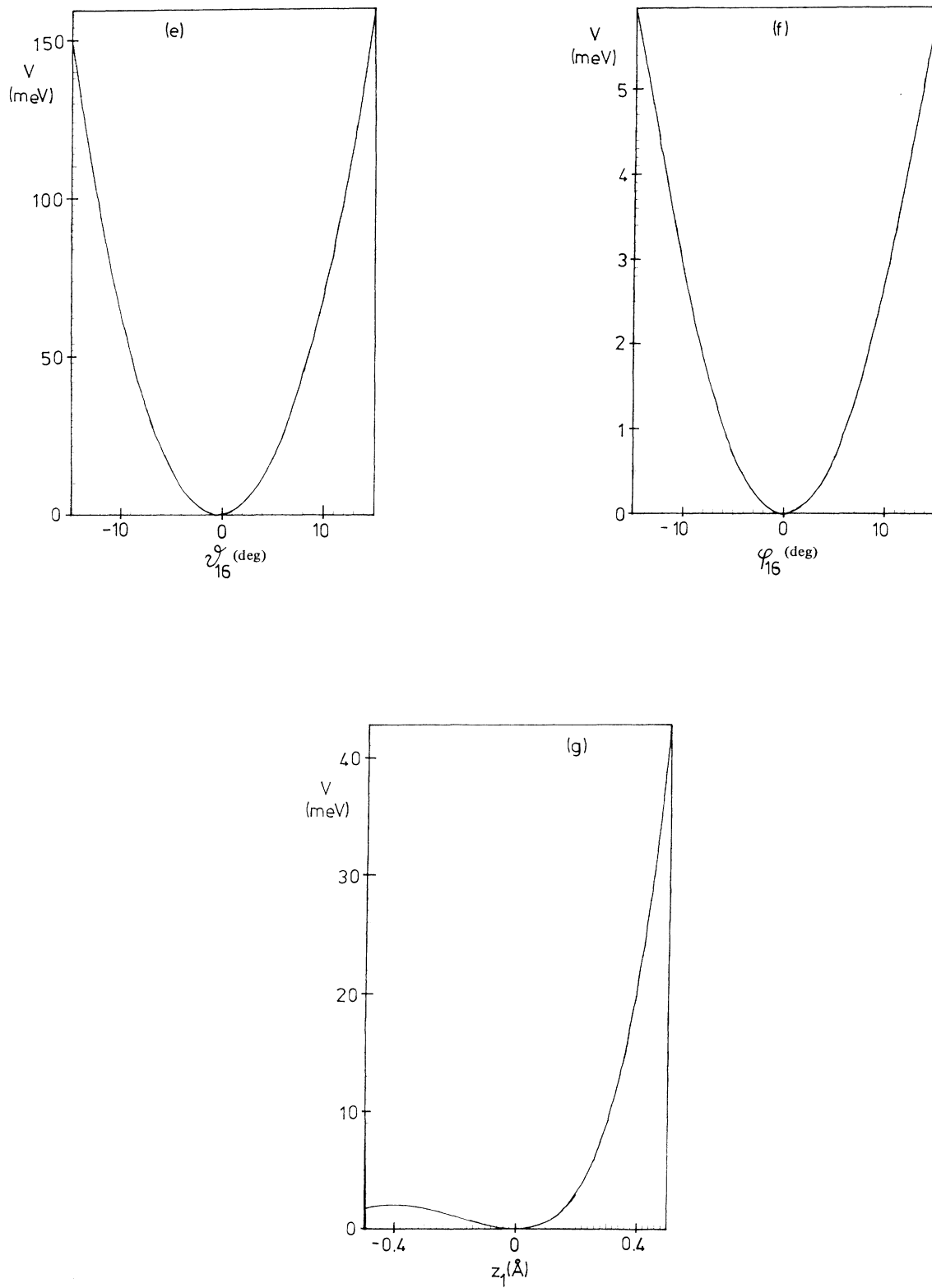


FIG. 6. (Continued).

potential $V_B^{(2)}$ is not too important for soliton formation, unless $V_B^{(2)}$ is larger than a certain threshold. In our case this threshold occurs between $0.01V_B^{(2)}$ and $0.05V_B^{(2)}$.

B. Dispersion energy

For a stack of 31 units we have computed the potential energy as function of the coordinates of the central unit (16). In Figs. 6(a)–6(c) the contributions of the dispersion energy E_D calculated with London's formula to the potential as function of z_{16} are shown. In Fig. 6(a) the first neighbors' term $E_D^{(1)}$, in Fig. 6(b) the second neighbors' term $E_D^{(2)}$, and in Fig. 6(c) the third neighbors' term $E_D^{(3)}$ is shown. Obviously $E_D^{(2)}$ is two, and $E_D^{(3)}$ three orders of magnitude smaller than $E_D^{(1)}$. Thus the dispersion energy contributions $E_D^{(n)}$ with $n \geq 2$ can be neglected. The dispersion energy curves as functions of ϑ_{16} and φ_{16} are very similar. Thus we include in our calculations only the first neighbor dispersion energy. In Figs. 6(d)–6(f) we show the total potential energy $V = V_{\text{HF}} + E_D^{(1)} + V_B$ (see Appendix B for the backbone term V_B) as a function of z_{16} [Fig. 6(d)], ϑ_{16} [Fig. 6(e)], and φ_{16} [Fig. 6(f)]. Obviously there is a rather strong dependence of V on ϑ_n and z_n but only a weak dependence on φ_n . In Fig. 6(e) we show $V(z_1)$ where the linear backbone potential terms, introduced to stabilize the chain, are included. Obviously there occurs a maximum at $z_1 \approx -0.4 \text{ \AA}$ and the barrier is only $\approx 2 \text{ meV}$. Thus the linear potential in case of dispersion is not sufficient to stabilize the chain. Therefore, we use fixed chain ends in all our simulations. An alternative to that would be a closed ring. However, in this case, as discussed below, from each excitation two waves would be emitted. Thus we prefer the fixed chain ends model.

To study the errors introduced by use of $V_D(\text{fit})$ we have computed soliton dynamics in a stack of 50 units using an excitation of $z_{49} = -0.4 \text{ \AA}$ and fixed chain ends as well as both $V_D(\text{fit})$ and V_D . In Table III the initial excitation energy $V^{(0)}$, mean kinetic energy \bar{T} , the time t_0 , the solitary wave needs to travel once through the stack, its velocity v_s , and its kinetic mass m^* (for calculation of

m^* it is assumed that \bar{T} corresponds to the kinetic energy of the wave) as function of z_{49} are given. Obviously $V_D(\text{fit})$ gives correct velocities and excitation energies. However, kinetic energy and thus kinetic mass is overestimated. But the approximate potential $V_D(\text{fit})$ can be used to obtain qualitative information about solitary waves. Especially for studies on our model systems $V_D(\text{fit})$ seems to be of sufficient accuracy. However, for future studies on realistic nucleotide base stacks one has to use London's formula explicitly. For $-0.2 \text{ \AA} < z_{49} < 0.2 \text{ \AA}$ no solitary waves are observed. In these low-energy cases the energy is distributed uniformly on the chain.

A striking difference between the two potentials occurs for $z_{49} = -0.4 \text{ \AA}$, shown in Fig. 7. In case of $V_D(\text{fit})$, Fig. 7(a), a solitary wave travels through the chain, however, a considerable part of the excitation energy remains in an oscillation at the chain end. In Figs. 7(b) the usual high-frequency oscillations in $T(t)$ (see Sec. III A) are seen and a minimum at the reflection from the chain end. Figure 7(d) (London's formula) shows oscillations which are much slower and three sharp minima at the two reflections and at the collision. Figure 7(c) computed with London's formula is strikingly different from Fig. 7(a). The excitation at z_{49} emits first the same solitary wave as seen in Fig. 7(a). But in this case two waves are emitted. The second one is immediately reflected at z_{50} and then follows the first one. Using $V_D(\text{fit})$ [Fig. 7(a)] the second wave is trapped. The difference between $z_{49} = +0.4 \text{ \AA}$ and $z_{49} = -0.4 \text{ \AA}$ is obvious. In the former case molecule 49 is shifted towards the fixed end molecule and by oscillating back emits the solitary wave. In the latter case molecule 49 is shifted towards the free molecule 48. This is repelled and the first solitary wave starts to travel. However, by oscillating back molecule 49 emits the second wave which is immediately reflected. Note that in case of $z_{49} = -0.3 \text{ \AA}$ both models give two solitary waves. Thus $V_D(\text{fit})$ can be safely used for small excitations as expected.

In Table IV we show soliton properties as function of chain length N after an excitation $z_{N-1} = +0.4 \text{ \AA}$ using

TABLE III. Initial excitation energy $V^{(0)}$, mean kinetic energy \bar{T} , time t_0 the solitary wave needs to pass once through the stack (50 units, ends fixed), velocity v_s of the wave, and its kinetic mass m^*/m_e as function of the initial excitation z_{49} , computed with sixth-order fit of the dispersion energy ("fit") and directly with London's formula ("London").

z_{49} (Å)	$V^{(0)}$ (meV)	\bar{T} (meV)	fit ^a			London ^a				
			t_0 (ps)	v_s (km/s) ^b	m^*/m_e	$V^{(0)}$ (meV)	\bar{T} (meV)	t_0 (ps)	v_s (km/s) ^b	m^*/m_e
-0.4 ^c	23.06	16.95	8.1	1.95	784	23.10	12.99	8.0	1.97	589
-0.3 ^d	10.66	7.95	9.0	1.75	457	10.86	5.47	9.0	1.75	314
0.2 ^e	4.02	4.25	9.8	1.61	288					
0.3	10.66	7.92	8.5	1.86	403	10.86	5.82	8.5	1.86	296
0.4	23.06	15.21	7.5	2.11	601	23.10	13.52	7.5	2.11	534

^aCPU time $t_{\text{London}}^{\text{CPU}}/t_{\text{fit}}^{\text{CPU}} = 1.48$; m_e : electron mass.

^bThe distance is equal to 47 unit distances which is 157.92 Å.

^cWhile for direct use of London's formula two solitary waves are emitted, in case of the fit one of them is trapped at the chain end.

^dIn both cases two waves are emitted; for $z = -0.2 \text{ \AA}$ and smaller no solitary wave is present.

^eCalculation with explicit formula not performed. In case of fit negative potential energies occur.

$V_D(\text{fit})$. Obviously for $N=50$ and 60 the kinetic energy \bar{T} , the velocity of the solitary wave, and its kinetic mass can be regarded as converged with respect to N . Therefore we use $N=50$ for our further calculations. For comparison between solitons in the simple Hartree-Fock potential (V_{HF}) model and in the models introduced here,

namely, $V_D(\text{fit})$ and V_D , we use the more interesting case of soliton collisions with initial excitations $z_2 = -0.4 \text{ \AA}$ and $z_{49} = 0.3 \text{ \AA}$. In Table V the soliton properties obtained from these calculations are listed, where the \bar{T} values for the single solitons are taken from extra calculations for these solitons. Obviously the excitation energy

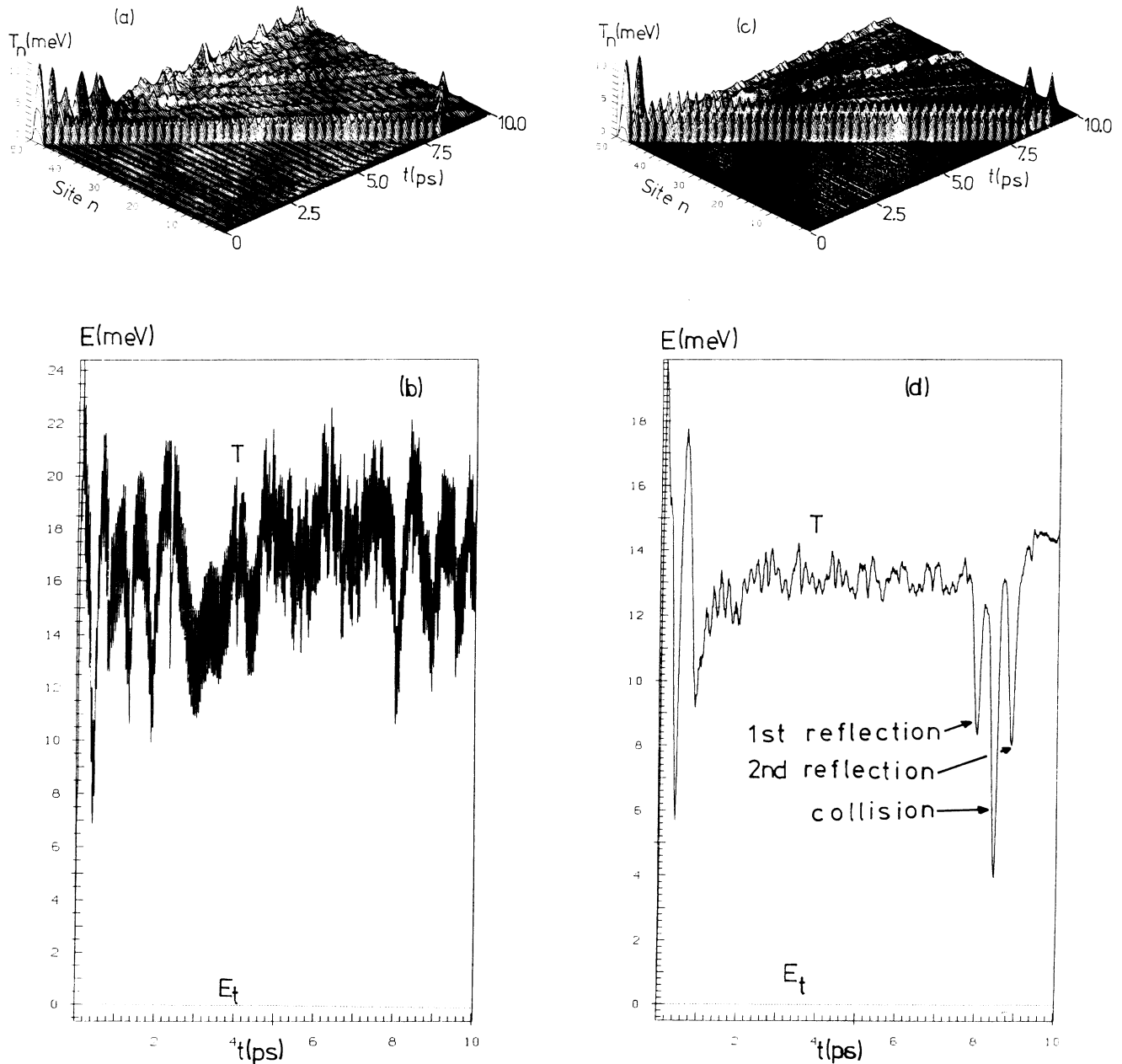


FIG. 7. Time evolution of a stack of 50 units after initial excitation $z_{49} = -0.4 \text{ \AA}$ using fixed chain ends. (a) Local kinetic energy T_n as function of time (t) and site (n) using $V_D(\text{fit})$; (b) kinetic energy T and total energy E_t (relative to $t=0$) as function of time (t) using $V_D(\text{fit})$; (c) same as (a), using V_D ; and (d) same as (b), using V_D .

TABLE IV. Mean kinetic energy \bar{T} , chain length R_0 , time t_0 the solitary wave needs to pass R_0 , its velocity v_s , and kinetic mass m^*/m_e (m_e is the electron mass) as function of the chain length N for an initial excitation $z_{N-1} = +0.4 \text{ \AA}$ ($V^{(0)} = 23.06 \text{ meV}$) and fixed chain ends, using the sixth-order fit for the dispersion energy.

N	\bar{T} (meV)	R_0 (Å)	t_0 (ps)	v_s (km/s)	m^*/m_e
20	13.73	57.12	3.1	1.84	713
40	14.76	124.32	6.1	2.04	624
50	15.21	157.92	7.5	2.11	611
60	15.47	191.52	9.0	2.13	600

TABLE V. Comparison of soliton properties using the potentials V_{HF} , $V_D(\text{fit})$, and V_D (see text for explanation) computed for the case of two solitons in a 50-unit stack [initial excitations $z_2 = -0.4 \text{ \AA}$ (I) and $z_{49} = 0.3 \text{ \AA}$ (II)].

Property	Soliton	V_{HF}	$V_D(\text{fit})$	V_D
$V^{(0)}$ (meV)	I+II	76.1	33.8	34.0
\bar{T} (meV)	I+II	42.3	20.9	19.3
	I	27.7	15.2	13.5
	II	14.6	7.9	5.8
v_s (km/s)	I	2.8	2.1	2.1
	II	2.6	1.9	1.9
m^*/m_e	I	1270	601	534
	II	790	403	296

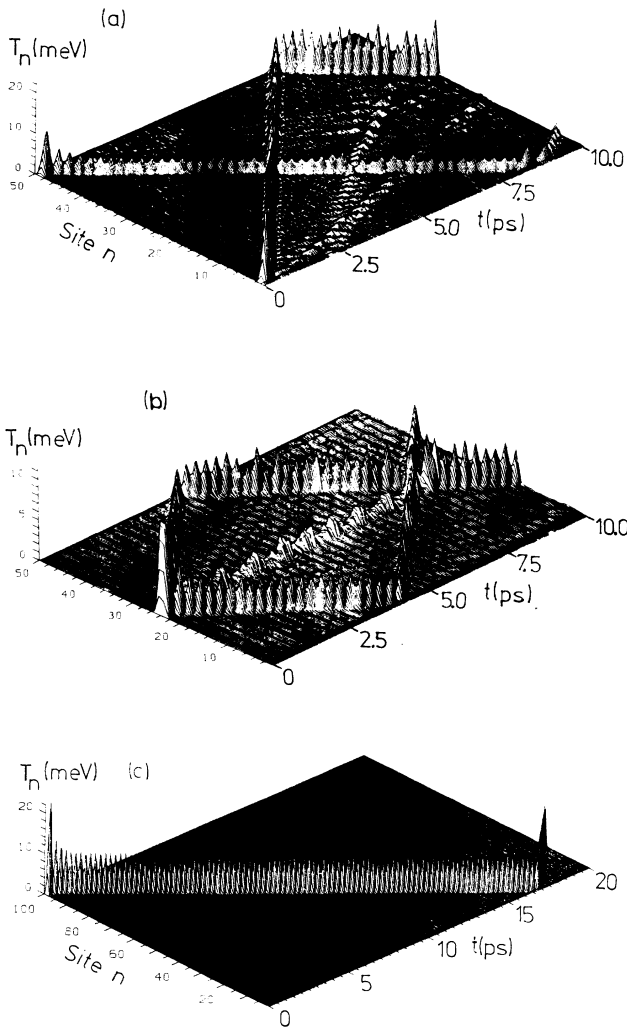


FIG. 8. Local kinetic energy T_n as function of time (t) and site (n) using fixed chain ends for different potentials, chain lengths N , and initial excitations [the case of V_{HF} is shown in Fig. 2(d)]. (a) $z_2 = -0.4 \text{ \AA}$, $z_{49} = 0.3 \text{ \AA}$, $N = 50$, V_D ; (b) $z_{24} = -z_{25} = 0.2 \text{ \AA}$, $N = 50$, $V_D(\text{fit})$; (c) $z_{49} = -0.4 \text{ \AA}$, $N = 100$, $V_D(\text{fit})$.

$V^{(0)}$ is decreased by a factor of 2 due to the dispersion energy. The same happens to the kinetic energy \bar{T} . While in case of V_{HF} and $V_D \bar{T}$ of the composite system is exactly the sum of \bar{T} from the single soliton calculations this is not exactly true for $V_D(\text{fit})$. The soliton velocities v_s are reduced upon inclusion of dispersion energy. The same

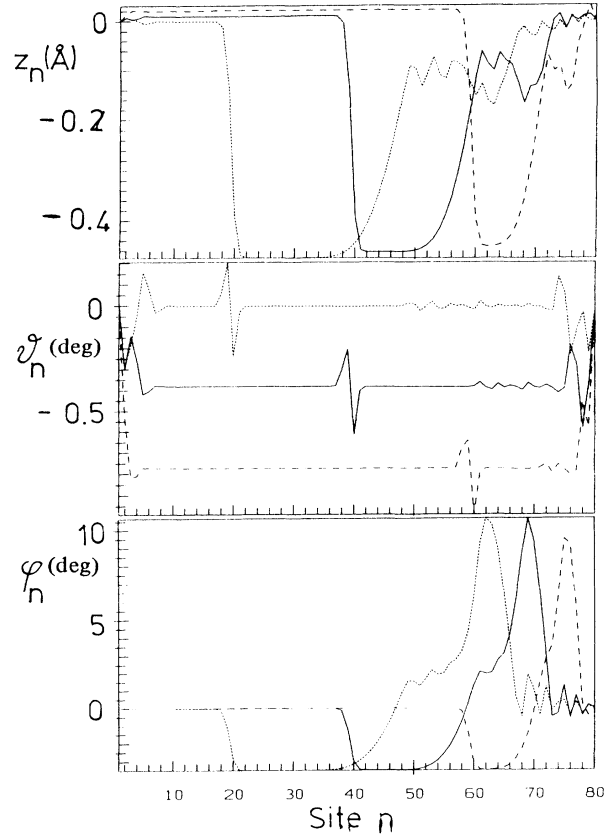


FIG. 9. The coordinates z_n , ϑ_n , and φ_n as functions of site n in a stack of 80 units after an initial excitation of $z_{79} = -0.4 \text{ \AA}$, using $V_D(\text{fit})$ and fixed chain ends at 3.25 ps (---), 6.25 ps (—), and 9.25 ps (- · - ·).

holds for the kinetic mass m^* . However, while $V_D(\text{fit})$ reproduces the velocities exactly, it overestimates the kinetic energy and kinetic mass of the waves considerably compared to V_D .

In Fig. 8 we show T_n as a function of time and site for some soliton simulations. In Fig. 8(a) the case $z_2 = -0.4 \text{ \AA}$ and $z_{49} = 0.3 \text{ \AA}$ is shown for V_D . In these cases and for V_{HF} [see Fig. 2(d)] the solitons penetrate each other undisturbed.

In Fig. 8(b) we show T_n as a function of site and time for the more important case of an excitation in the center of the chain, using $V_D(\text{fit})$. Figure 8(b) shows the case of $z_{24} = -z_{25} = 0.2 \text{ \AA}$. Here two waves are emitted but a part of the excitation energy is trapped in an oscillation in the center of the chain. However, this may well be an artifact of $V_D(\text{fit})$.

In Fig. 8(c) we show T_n as function of site and time in a large stack of 100 units after initial excitation of $z_{99} = -0.4 \text{ \AA}$. In this simulation the solitary character of the wave can be seen. After some initial relaxation the height of the narrow peak does not change in time. Also its width remains unchanged. Even after reflection the wave is unperturbed. Figure 8(c) suggests that the wave could travel through even much longer chains than 100 units (336 \AA) without any visible broadening.

Finally in Fig. 9 we show z_n , ϑ_n , and φ_n as function of n for three different times in a stack of 80 units. In contrast to the local kinetic energy the geometrical distortion broadens somewhat with time. In case of z_n the width of the distortion increases from ≈ 6 sites at 3.25 ps through ≈ 12 sites at 6.25 ps to ≈ 20 sites at 9.25 ps. This distortion in the z_n is followed by a very narrow and small distortion in ϑ_n . The distortion in the φ_n has almost the same shape as that in the z_n but is followed by a slow and sharp peak. In the kinetic energy the soliton manifests itself as a very narrow energy packet. This corresponds to the sharp change in z_n from 0.0 to -0.4 \AA within roughly four lattice sites. The relaxation of the distortion, however, is connected with a very small kinetic energy and thus occurs very slowly.

IV. CONCLUSION

We have introduced and applied the exact equations of motion for the dynamics of stacked systems. Significant differences to the results obtained previously in an approximate version of the equations are reported. Especially it turned out that for more realistic potential functions (introducing also a backbone potential holding together the stack) than previously used only application of the exact equations of motion leads to solitary waves. Potential functions of this kind depend not only on the coordinate differences $\Delta \mathbf{q}_n$ but also on the coordinates \mathbf{q}_n themselves. They necessarily occur if the backbone is included in a more realistic way, in case of hydrogen bonds in double helices, and also if higher energy excitations should be considered. Thus incorporation of the exact equations of motion into the model is an important step before realistic systems like DNA stacks which exhibit the above-mentioned features can be treated.

Further we have introduced the intermolecular disper-

sion energy using London's formula into our model for soliton dynamics in stacked systems. It was shown that second-neighbor dispersion energy terms are already negligible. The dispersion energy can be expanded into a Taylor series as the Hartree-Fock potential if only qualitative conclusions are desired. For quantitative calculations, high-energy excitations, and in realistic systems the explicit use of London's formula is indispensable. Upon inclusion of dispersion energy excitation energies, kinetic energies, soliton velocities and kinetic masses are considerably reduced compared to a HF potential. Thus the inclusion of dispersion energy into a realistic model is of utmost importance. We found solitary waves emitted from excitations at the chain ends as well as from central excitations. They carry roughly $\frac{2}{3}$ of the initial excitation energy through the stack. The solitary waves penetrate each other unperturbed and are able to travel through long segments of the stack ($N > 100$).

As the next step we show in paper II that electron-electron interaction need not be included explicitly into the model. Calculations on the influence of impurities on soliton dynamics have been published elsewhere.³² After completion of these model investigations one is in a position to investigate the more complex, but realistic problem of DNA. In this case environmental effects have to be included using random forces and dissipation terms. Finally, we want to mention that the kinetic masses of the soliton in these stacked systems are rather large ($> 100m_e$). Therefore the use of quantum equations of motion most probably will not be necessary. However, this has to be shown by numerical calculations.

ACKNOWLEDGMENTS

The financial support of the "Deutsche Forschungsgemeinschaft" (Project No. Ot 51/6-1), of the National Foundation for Cancer Research, and of the "Fond der Chemischen Industrie" is gratefully acknowledged.

APPENDIX A: CORRECTIONS TO THE HARTREE-FOCK POTENTIAL

The potential V applied in our calculations consists (ignoring the dispersion term) basically of two different parts, namely, the Hartree-Fock potential V_{HF} and a correction V_B which is due to the backbone which exists in realistic DNA stacks. The construction of V_{HF} is extensively described in Ref. 16 so we do not want to discuss it at this point. V_{HF} of a stack is written as a sum of pair potentials, where the constants K_{ijk} were determined as described in Ref. 16:

$$V_{\text{HF}} = \sum_{i,j,k \geq 0}^{i+j+k \leq 6} K_{ijk} \sum_{n=1}^{N-1} \Delta z_n^i \Delta \vartheta_n^j \Delta \varphi_n^k, \quad (\text{A1})$$

where

$$\Delta \mathbf{q}_n = \mathbf{q}_{n+1} - \mathbf{q}_n, \quad \mathbf{q}_n^+ \equiv (z_n, \vartheta_n, \varphi_n). \quad (\text{A2})$$

Ansatz (A1) contains an approximation which deserves some discussion. Namely, while the dimer energy is only a function of Δz and $\Delta \varphi$ and not of the individual coordi-

nates, for ϑ and the energy depends on both ϑ_1 and ϑ_2 and not only on $\Delta\vartheta$. In Table VI in columns 7 and 8 we give the directly computed HF energies [using the GAUSSIAN 74 (Ref. 29) program] and those obtained from our fit compared to the case of $\Delta z = \Delta\vartheta = \Delta\varphi = 0$ in meV for a number of dimer geometries. We give six groups of geometries where within a group $\Delta\vartheta$ is the same but the individual ϑ_1 and ϑ_2 values are different. Thus our fit (column 8) gives the same energy within such groups. The last two groups contain the maximal possible values of Δz and $\Delta\varphi$ for the sake of comparison. Obviously the error introduced by the assumption that the energy depends only on $\Delta\vartheta$ is $\approx 6-10\%$ for high-energy geometries (> 50 meV) and $\approx 4\%$ for low-energy geometries. Thus for our model studies with low-energy excitations the approximation that one takes into account only $\Delta\vartheta$ seems to be justified. However, it is also obvious that for more realistic calculations on DNA stacks with high-energy excitations a Taylor-series expansion in four variables ($\Delta z, \vartheta_1, \vartheta_2, \Delta\varphi$) has to be used. Also the range of the fit has to be extended. Calculations along these lines are already in progress.

One can see that in our minimal basis-set calculations the basis-set superposition error (BSSE) plays an important role. Therefore interaction energies are in general too small. In the fifth column of Table VI we give the interaction energies V_{HF}^I computed in this way for the dimer geometries listed. A usual way to correct this error is the counterpoise correction, where also in the monomer calculations the full basis set of the dimers is applied. The sixth column of Table VI gives the corrected energies $V_{\text{HF}}^I(\text{BSSE})$ obtained in this way. However, the counterpoise correction overestimates the BSSE, since now the variational spaces for the electrons in the monomer calculations are too large. As Table VI shows the BSSE in our calculations is rather large, and moreover does not lead to the same upward shift of all interaction energies. However, for our purpose the interaction energies are unimportant. We are only interested in the energy of a given dimer with respect to the reference geometry ($\Delta z = \Delta\vartheta = \Delta\varphi = 0$). Thus the large BSSE does not affect the results of our dynamical simulations.

Let us now turn to the ‘‘backbone’’ term V_B . Its introduction is necessary because neither formamide nor nu-

TABLE VI. Interaction energy (in meV) in a formamide dimer computed with the *ab initio* Hartree-Fock method (V_{HF}^I) and corrected against basis set superposition error [$V_{\text{HF}}^I(\text{BSSE})$] as well as energies relative to the equilibrium energy computed with the Hartree-Fock method (V_{HF}) and with our sixth-order Taylor series [$V_{\text{HF}}(\text{fit})$] for different geometries ($\Delta z, \vartheta_1, \vartheta_2, \Delta\varphi$).

Δz (Å)	ϑ_1 (°)	ϑ_2 (°)	$\Delta\varphi$ (°)	V_{HF}^I	$V_{\text{HF}}^I(\text{BSSE})$	V_{HF}	$V_{\text{HF}}(\text{fit})^a$
0	0	0	0	40.65	49.71	0.0 ^b	
0	7.5	7.5	0	40.07	49.77	-0.58	0.0 ^c
0	-7.5	-7.5	0	40.79	50.36	+0.14	
0	-15.0	0	0	26.84	29.41	-13.81	
0	-7.5	7.5	0	27.12	29.49	-13.53	-13.37(3.3%)
0	0	15.0	0	26.99	29.50	-13.66	
0	+15.0	0	0	99.72	142.07	59.07	
0	7.5	-7.5	0	97.94	137.50	57.29	55.35(6.7%)
0	0	-15.	0	96.06	136.15	55.44	
-0.5	+15.0	0	0	596.37	808.86	555.72	
-0.5	7.5	-7.5	0	566.16	769.90	525.51	506.36(9.8%)
-0.5	0.	-15.0	0	549.07	752.86	508.42	
0	15.0	0	-15.0	153.86	205.19	113.21	
0	7.5	-7.5	-15.0	151.07	202.23	110.42	102.84(10.1%)
0	0	-15.	-15.0	142.83	197.27	102.18	
-0.5	15.0	0	-15.0	872.63	1133.08	831.98	
-0.5	7.5	-7.5	-15.0	859.69	1122.42	819.04	774.73(7.4%)
-0.5	0	-15.	-15.0	842.19	1114.87	801.54	
0.5	0	0	0	146.04	203.48	105.39	105.43
-0.5	0	0	0	23.70	24.74	-16.95	-16.96
0	0	0	15.0	29.39	36.77	-11.26	-11.25
0	0	0	-15.0	56.60	67.45	15.59	16.31

^aNumbers in parentheses indicate the maximum errors in percent of $V_{\text{HF}}(\text{fit})$.

^bEquilibrium dimer energy: -333.359 327 hartree.

^cEquilibrium dimer energy: -333.359 332 hartree.

TABLE VII. The coefficients B_ν (in eV/(Rad) $^\nu$) for the polynomial applied in the backbone potential $V_B^{(2)}$.

ν	B_ν (eV/rad $^\nu$)	ν	B_ν (eV/rad $^\nu$)
0	0.	6	-300.7116
1	0.0265	7	-17.3695
2	1.9577	8	11 314.8551
3	-0.0992	9	214.5970
4	4.4574	10	-188 315.5451
5	0.6961	11	-1090.5620
		12	1.1227×10^6

cleotide base stacks are stable in themselves in the geometry of B-DNA.³⁰ The most simple way to construct such a potential $V_B^{(1)}$ is to use a linear ansatz for it

$$V_B^{(1)} = \sum_{n=1}^{N-1} (A_z \Delta z_n + A_\vartheta \Delta \vartheta_n + A_\varphi \Delta \varphi_n), \quad (\text{A3})$$

where the constants $A_z, A_\vartheta, A_\varphi$ are chosen in such a way that the first derivatives of the total potential in a predefined “equilibrium” geometry are zero (see Ref. 16). In this way $V_B^{(1)}$ contains only a minimum of information about the real backbone, namely, that it stabilizes the “equilibrium” geometry. Since in (A3) most terms cancel $V_B^{(1)}$ simplifies to

$$V_B^{(1)} = A_z(z_N - z_1) + A_\vartheta(\vartheta_N - \vartheta_1) + A_\varphi(\varphi_N - \varphi_1) \quad (\text{A4})$$

for a stack of N molecules. Therefore an alternative way to stabilize the equilibrium geometry would be simply to fix the two molecules at the two ends of the stack.

However, as discussed in Appendix C for our case at least for the angle ϑ information about the form of the backbone potential is necessary since in case of ϑ the results depend qualitatively on the presence of the potential term $V_B^{(2)}$. To obtain a rough estimate of such a potential we have computed the energy of the molecule shown in Fig. 10 as function of ϑ where ϑ corresponds to the rotation around the z axis leaving the CH_3 group (z is in this figure not the direction perpendicular to the stack) un-

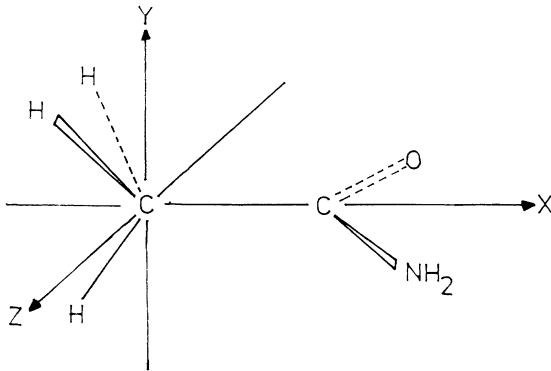


FIG. 10. Sketch of the molecule used for calculation of the $V_B^{(2)}$ backbone potential.

TABLE VIII. Nuclear repulsion (E_n), electronic (E_e), and total energy (E_t) (all in hartrees) for a stack of three units and a tilting angle of $\vartheta = \pm 10^\circ$ of the center molecule as well as the differences $\Delta E = E_{10} - E_{-10}$ between these energies, calculated with a minimal basis set.

Energy type	$\vartheta = 10^\circ$	$\vartheta = -10^\circ$	ΔE
E_n	+412.337 839	+412.227 592	+2.9998 eV
E_e	-912.375 434	-912.265 203	-2.9994 eV
E_t	-500.037 595	-500.037 611	+0.4354 meV

changed. This is only a first estimate for $V_B^{(2)}$ since the sugar-phosphate group in the real DNA backbone is far more flexible than the rigid CH_3 group applied here. However, for our model calculation such an estimate seems to be sufficient. The energy has been computed for 13 values of ϑ within $-15^\circ \leq \vartheta \leq 15^\circ$ and a polynomial of 12th degree has been adjusted to them leading to

$$V_B^{(2)} = \sum_n \sum_{\nu=0}^{12} B_\nu \vartheta_n^\nu. \quad (\text{A5})$$

The coefficients B_ν are given in Table VII. The small term B_1 leads to a slight shift of the equilibrium geometry. However, since $\theta^{(e)} < 1^\circ$ this shift is unimportant. Although B_{12} seems to be rather large, one should keep in mind that even for the largest possibly occurring value $\vartheta = 15^\circ$, its contribution to $V_B^{(2)}$ is only 0.12 eV. Thus

$$V_B = V_B^{(1)} + V_B^{(2)} \quad (\text{A6})$$

is the complete backbone potential applied in this case.

If one considers a system of three units and looks at the HF-potential energy as function of ϑ of the molecule in the middle, one may expect that the symmetry $V(\vartheta) = V(-\vartheta)$ occurring in our potential ansatz is not realistic. Therefore we show in Table VIII the nuclear, electronic, and total energy of this system for $\vartheta = 10^\circ$ and -10° . Obviously nuclear and electronic energies of the system are different. However, their sums are in a very good approximation the same in both cases giving a nearly constant total energy (see Table IX).

APPENDIX B: RELATIONS BETWEEN EXACT AND APPROXIMATE EQUATIONS OF MOTION

In this appendix we want to discuss in some more detail which approximations lead from the exact equations of motion described here to the more simple ones used in Ref. 16. First of all, in the simpler equations $z, \vartheta,$ and φ are treated as independent coordinates. Thus they can be approximately correct only for small values of ϑ , ideally for $\vartheta = 0$. Putting $\vartheta = 0$, in the equations of motion [(14), (22), and (24)] we obtain the approximate equations

$$M\ddot{z}_n + M_x \ddot{\vartheta}_n + M_z \dot{\vartheta}_n^2 = - \frac{\partial V}{\partial z_n}, \quad (\text{B1})$$

$$M_x \ddot{z}_n + (M_{xx} + M_{zz}) \ddot{\vartheta}_n + M_{yz} \ddot{\varphi}_n - M_{xz} \dot{\varphi}_n^2 = - \frac{\partial V}{\partial \vartheta_n}, \quad (B2)$$

$$M_{xy} \ddot{\vartheta}_n + (M_{xx} + M_{yy}) \ddot{\varphi}_n + 2M_{xz} \dot{\vartheta}_n \dot{\varphi}_n - M_{xy} \dot{\vartheta}_n^2 = - \frac{\partial V}{\partial \varphi_n}. \quad (B3)$$

From the geometry of our model system it follows that $M_z = M_{zz} = M_{yz} = 0$. Further $M_{xx} + M_{zz} = \theta_\vartheta$ and $M_{xx} + M_{yy} = \theta_\varphi$ (in the $\vartheta=0$ approximation). Thus (B1)–(B3) reduce to

$$M \ddot{z}_n + M_x \ddot{\vartheta}_n = - \frac{\partial V}{\partial z_n}, \quad (B4)$$

$$M_x \ddot{z}_n + \theta_\vartheta \ddot{\vartheta}_n = - \frac{\partial V}{\partial \vartheta_n}, \quad (B5)$$

$$\theta_\varphi \ddot{\varphi}_n - M_{xy} \dot{\vartheta}_n^2 = - \frac{\partial V}{\partial \varphi_n}. \quad (B6)$$

Obviously the $\vartheta=0$ approximation is not sufficient to obtain the simple equations of motion used in Ref. 16. Obviously

$$M_x = \sum_i m_i x_{i0} = MR_x, \quad (B7)$$

where m_i are the masses and x_{i0} the x coordinates of the atoms in the reference geometry, and R_x is the x coordinate of the center of mass. Therefore the simple equations of motion assume further that the rotation axis for ϑ contains the center of mass of the molecule which is not the case in our system. The other additional term in (B6) contains $-M_{xy}$ which is one of the so-called products of inertia. The occurrence of this term is due to the fact that the coordinate system is not oriented parallel to the main axes of the tensor of inertia, i.e., this tensor is not diagonal in the reference geometry. Thus if we further assume that the molecule is situated with its center of mass in the origin of the coordinate system and oriented such that the main axes of its tensor of inertia are parallel to the coordinate axes we obtain the equations of motion used in Ref. 16 from (B4)–(B6):

$$M \ddot{z}_n = - \frac{\partial V}{\partial z_n}, \quad \theta_\vartheta \ddot{\vartheta}_n = - \frac{\partial V}{\partial \vartheta_n}, \quad \theta_\varphi \ddot{\varphi}_n = - \frac{\partial V}{\partial \varphi_n}. \quad (B8)$$

APPENDIX C: CONSTANTS OF MOTION

As obvious from (B8) the constants of motion for the approximate equations are total energy, total momentum P

$$P = M \sum_{n=1}^N \dot{z}_n, \quad (C1)$$

and total angular momenta L_ϑ, L_φ

$$M \sum_n \dot{z}_n + M_z \sum_n (\dot{\vartheta}_n \sin \vartheta_n + \dot{\vartheta}_n^2 \cos \vartheta_n) + M_x \sum_n (\dot{\vartheta}_n \cos \vartheta_n - \dot{\vartheta}_n^2 \sin \vartheta_n) = 0 \quad (C12)$$

$$L_\theta = \theta_\vartheta \sum_{n=1}^N \dot{\vartheta}_n, \quad L_\varphi = \theta_\varphi \sum_{n=1}^N \dot{\varphi}_n. \quad (C2)$$

In case of the exact equations of motion it is more difficult to derive the conserved quantities. Since the Lagrange function L is not explicitly dependent on time t , i.e., $L = L(\mathbf{q}_n, \dot{\mathbf{q}}_n)$, the total energy is conserved³¹

$$\frac{d}{dt} L = \sum_{n,\mu} \left[\frac{\partial L}{\partial q_{n\mu}} \dot{q}_{n\mu} + \frac{\partial L}{\partial \dot{q}_{n\mu}} \ddot{q}_{n\mu} \right], \quad \mu = 1, 2, 3. \quad (C3)$$

From the Lagrange equations we know that

$$\frac{\partial L}{\partial q_{n\mu}} = \frac{d}{dt} \frac{\partial L}{\partial \dot{q}_{n\mu}}. \quad (C4)$$

Thus together with (C3) one obtains

$$\begin{aligned} \frac{d}{dt} L &= \sum_{n,\mu} \left[\dot{q}_{n\mu} \frac{d}{dt} \frac{\partial L}{\partial \dot{q}_{n\mu}} + \frac{\partial L}{\partial \dot{q}_{n\mu}} \frac{d}{dt} \dot{q}_{n\mu} \right] \\ &= \frac{d}{dt} \sum_{n,\mu} \frac{\partial L}{\partial \dot{q}_{n\mu}} \dot{q}_{n\mu} \end{aligned} \quad (C5)$$

and hence

$$\frac{d}{dt} \left[\sum_{n,\mu} \frac{\partial L}{\partial \dot{q}_{n\mu}} \dot{q}_{n\mu} - L \right] = 0. \quad (C6)$$

Since $V = V(\mathbf{q}_n)$ and independent of $\dot{\mathbf{q}}_n$ or t one can write

$$\begin{aligned} \sum_{n,\mu} \frac{\partial L}{\partial \dot{q}_{n\mu}} \dot{q}_{n\mu} &= \sum_{n,\mu} \frac{\partial T_n}{\partial \dot{q}_{n\mu}} \dot{q}_{n\mu} \\ &= \frac{1}{2} \sum_{n,\mu} \dot{q}_{n\mu} \frac{\partial}{\partial \dot{q}_{n\mu}} (\dot{\mathbf{q}}_n^+ \underline{\mathbf{K}}_n \dot{\mathbf{q}}_n) \\ &= \sum_n \dot{\mathbf{q}}_n^+ \underline{\mathbf{K}}_n \dot{\mathbf{q}}_n = 2T. \end{aligned} \quad (C7)$$

Together with (C6) and $L = T - V$ we obtain

$$\frac{d}{dt} (T + V) = 0 \quad (C8)$$

and thus—as expected—the total energy is conserved.

If $V_B^{(2)} = 0$, and thus $V = V(\Delta \mathbf{q}_n)$ one can derive other conserved quantities, by using

$$\frac{\partial V}{\partial q_{n\mu}} = - \frac{\partial V}{\partial \Delta q_{n\mu}} (1 - \delta_{n,N}) + \frac{\partial V}{\partial \Delta q_{n-1,\mu}} (1 - \delta_{n,1}). \quad (C9)$$

Then our equations of motion are

$$\underline{\mathbf{K}}_n \ddot{\mathbf{q}}_n + \mathbf{Q}_n = \frac{\partial V}{\partial \Delta \mathbf{q}_n} (1 - \delta_{n,N}) - \frac{\partial V}{\partial \Delta \mathbf{q}_{n-1}} (1 - \delta_{n,1}). \quad (C10)$$

Summation of Eqs. (C10) over n leads to

$$\sum_{n=1}^N (\underline{\mathbf{K}}_n \ddot{\mathbf{q}}_n + \mathbf{Q}_n) = 0. \quad (C11)$$

The first equation of (C11) can be written explicitly

or

$$M \sum_n \frac{d}{dt} \dot{z}_n + M_x \sum_n \frac{d}{dt} (\dot{\vartheta}_n \cos \vartheta_n) + M_z \sum_n \frac{d}{dt} (\dot{\vartheta}_n \sin \vartheta_n) = 0 \quad (\text{C13})$$

and thus

$$-\frac{d}{dt} P_z = 0, \quad (\text{C14})$$

where P_z is the z component of the total momentum, given by

$$P_z = -M \sum_n \dot{z}_n - \sum_n \dot{\vartheta}_n (M_x \cos \vartheta_n + M_z \sin \vartheta_n). \quad (\text{C15})$$

Thus in the exact case P_z is more complicated than in the approximate one since here also rotations around ϑ_n contribute to it. Note that conservation of P_z holds also for $V_B^{(2)} \neq 0$ because the dependence of V on z_n is not affected by $V_B^{(2)}$. That (C14) is correct can be most easily verified by calculating directly the z component of the center of mass of the stack and its total time derivative using Eqs. (1)–(3).

In the same way one can compute the z component L_z of the total angular momentum of the stack which is given by

$$L_z = - \sum_n [\dot{\varphi}_n (M_{yy} + M_{xx} \cos^2 \vartheta_n + M_{zz} \sin^2 \vartheta_n + 2M_{xz} \sin \vartheta_n \cos \vartheta_n) + \dot{\vartheta}_n (M_{yz} \cos \vartheta_n - M_{xy} \sin \vartheta_n)]. \quad (\text{C16})$$

Differentiation of (C16) with respect to time yields

$$\begin{aligned} \frac{d}{dt} L_z &= - \sum_n [K_n(3,2) \ddot{\vartheta}_n + K_n(3,3) \dot{\varphi}_n - \dot{\vartheta}_n^2 (M_{yz} \sin \vartheta_n + M_{xy} \cos \vartheta_n) - 2Y \dot{\varphi}_n \dot{\vartheta}_n] \\ &= - \sum_n \left[\sum_{\mu=1}^3 K_n(3,\mu) \ddot{q}_{n\mu} + Q_n(3) \right]. \end{aligned} \quad (\text{C17})$$

Since (C17) is nothing else than the negative of the third component of Eq. (C11) we have shown that

$$\frac{d}{dt} L_z = 0 \quad (\text{C18})$$

and therefore also the z component of angular momentum is conserved. Also (C18) holds if $V_B^{(2)} \neq 0$.

From the second component of (C11) another conserved quantity can be derived. However, this conservation holds only if $V_B^{(2)} = 0$. Therefore we do not want to elaborate on this here. We only want to mention that it is related to the conservation of L_ϑ in the approximate equations. Its nonconservation if $V_B^{(2)} \neq 0$ is due to the fact that a potential depending on \mathbf{q}_n and not on $\Delta \mathbf{q}_n$ is due to an external force, backbone or environment. However, until the system remains conservative the total energy is conserved in any case.

APPENDIX D: COMPUTATION OF DISTANCES BETWEEN ATOMS AND THEIR DERIVATIVES

In this appendix we would like to outline shortly the computation of the distances R_{gh}^{nm} between two atoms g and h in the formamide units n and m , respectively, as function of the coordinates \mathbf{q}_n and \mathbf{q}_m . Finally, the derivatives of the R_{gh}^{nm} with respect to the \mathbf{q}_m are given. Starting from the reference molecule (see Table IX for its coordinates) one obtains the position vector \mathbf{r}_{gn} of atom g in molecule n from the position vector \mathbf{r}_{g0} of g in the reference molecule from Eqs. (1)–(4) in Sec. II. Then the vector pointing from g to h is given by

$$\mathbf{R}_{gh}^{nm} = \mathbf{r}_{hm} - \mathbf{r}_{gn} \quad (\text{D1})$$

and

$$R_{gh}^{nm} = |\mathbf{r}_{hm} - \mathbf{r}_{gn}|. \quad (\text{D2})$$

This leads to

$$\begin{aligned} R_{gh}^{nm} &= [(\underline{D}'_m \mathbf{r}_{h0} - \underline{D}'_n \mathbf{r}_{g0})^2 \\ &\quad - 2(Z_m - Z_n)(\underline{D}'_m \mathbf{r}_{h0} - \underline{D}'_n \mathbf{r}_{g0}) \cdot \mathbf{e}_z \\ &\quad + (Z_m - Z_n)^2]^{1/2}. \end{aligned} \quad (\text{D3})$$

For the definition of \underline{D}'_n see Eqs. (2) and (3).

$X_{gn}^{\mu 1}$, the μ component ($\mu = x, y, z$) of \mathbf{x}_{gn} , is given by

$$\begin{aligned} X_{gn}^{11} &= x_{g0} \cos \phi_n \cos \vartheta_n + y_{g0} \sin \phi_n + z_{g0} \cos \phi_n \sin \vartheta_n, \\ X_{gn}^{21} &= -x_{g0} \sin \phi_n \cos \vartheta_n + y_{g0} \cos \phi_n - z_{g0} \sin \phi_n \sin \vartheta_n, \\ X_{gn}^{31} &= -x_{g0} \sin \vartheta_n + z_{g0} \cos \vartheta_n. \end{aligned} \quad (\text{D4})$$

TABLE IX. Cartesian coordinates of the reference molecule (in Å) (all z coordinates are 0).

Atom	No.	X	Y
H	1	0.0	0.0
C	2	1.08000	0.0
O	3	1.69000	1.05655
N	4	1.81500	-1.27306
H	5	2.82500	-1.27306
H	6	1.31000	-2.14774

Then one can write

$$R_{gh}^{nm} = \left[\sum_{\mu=1}^3 (X_{hm}^{\mu 1} - X_{gn}^{\mu 2})^2 - 2(Z_m - Z_n)(X_{hm}^{31} - X_{gn}^{31}) + (Z_m - Z_n)^2 \right]^{1/2}. \quad (D5)$$

If one defines

$$X_{gn}^{\mu 2} \equiv \frac{\partial}{\partial \vartheta_n} X_{gn}^{\mu 1}, \quad X_{gn}^{\mu 3} \equiv \frac{\partial}{\partial \varphi_n} X_{gn}^{\mu 1}, \quad (D6)$$

the straightforward differentiation of (D4) and (D5) leads finally to

$$\begin{aligned} \frac{\partial R_{gh}^{nm}}{\partial z_m} &= (-Z_m + Z_n + X_{hm}^{31} - X_{gn}^{31})(R_{gh}^{nm})^{-1}, \\ \frac{\partial R_{gh}^{nm}}{\partial \vartheta_m} &= \left[\sum_{\mu=1}^3 (X_{hm}^{\mu 1} - X_{gn}^{\mu 1})X_{hm}^{\mu 2} - (Z_m - Z_n)X_{hm}^{32} \right] (R_{gh}^{nm})^{-1}, \\ \frac{\partial R_{gh}^{nm}}{\partial \varphi_m} &= \left[\sum_{\mu=1}^3 (X_{hm}^{\mu 1} - X_{gn}^{\mu 1})X_{hm}^{\mu 3} - (Z_m - Z_n)X_{hm}^{33} \right] (R_{gh}^{nm})^{-1}. \end{aligned} \quad (D7)$$

- ¹H. J. Mikeska, *J. Phys. C* **11**, L29 (1978).
²K. Maki, *J. Low. Temp. Phys.* **41**, 327 (1980).
³K. J. Wahlstrand, *J. Chem. Phys.* **82**, 5257 (1985); K. J. Wahlstrand and P. G. Waylnes, *ibid.* **82**, 5259 (1985).
⁴S. Aubry, *J. Chem. Phys.* **64**, 3392 (1976); M. A. Collins, A. Blumen, J. F. Currie, and J. Ross, *Phys. Rev. B* **19**, 3630 (1979).
⁵W. P. Su, J. R. Schrieffer, and A. J. Heeger, *Phys. Rev. Lett.* **42**, 1698 (1979); W. P. Su, *Solid State Commun.* **35**, 899 (1980); W. P. Su, J. R. Schrieffer, and A. J. Heeger, *Phys. Rev. B* **22**, 2099 (1980); W. P. Su and J. R. Schrieffer, *Proc. Natl. Acad. Sci. U.S.A.* **77**, 5626 (1980); F. Guinea, *Phys. Rev. B* **30**, 1884 (1984); A. R. Bishop, D. K. Campbell, P. S. Lomdahl, B. Horowitz, and S. R. Phillpot, *Phys. Rev. Lett.* **52**, 671 (1984); W. Förner, M. Seel, and J. Ladik, *Solid State Commun.* **57**, 463 (1986); *J. Chem. Phys.* **84**, 5910 (1986); A. Godzik, M. Seel, W. Förner, and J. Ladik, *Solid State Commun.* **60**, 609 (1987); C.-M. Liegener, W. Förner, and J. Ladik, *Solid State Commun.* **61**, 203 (1987); S. R. Phillpot, D. Baeriswyl, A. R. Bishop, and P. S. Lomdahl, *Phys. Rev. B* **35**, 7533 (1987).
⁶S. Kivelson and D. E. Heim, *Phys. Rev. B* **26**, 4278 (1982); A. J. Heeger and J. R. Schrieffer, *Solid State Commun.* **48**, 207 (1983); Z. G. Soos and S. Ramasesha, *Phys. Rev. Lett.* **51**, 2374 (1983); H. Sasai and H. Fukutome, *Synth. Met.* **9**, 295 (1984); W. P. Su, *Phys. Rev. B* **34**, 2988 (1986); S. Kivelson and Wei-kang Wu, *ibid.* **34**, 5423 (1986).
⁷C. L. Wang and F. Martino, *Phys. Rev. B* **34**, 5540 (1986); W. Förner, C. L. Wang, F. Martino, and J. Ladik, *ibid.* **37**, 4567 (1988); W. Förner, *Solid State Commun.* **63**, 941 (1987); R. Markus, W. Förner, and J. Ladik, *ibid.* **63**, 135 (1988); H. Orendi, W. Förner, and J. Ladik, *Chem. Phys. Lett.* **150**, 113 (1988).
⁸A. S. Davydov and N. I. Kislukha, *Phys. Status Solidi B* **59**, 465 (1973); A. S. Davydov, *Phys. Scr.* **20**, 387 (1979); A. S. Davydov, *Usp. Fiz. Nauk* **138**, 603 (1982) [*Sov. Phys.—Usp.* **25**, 898 (1982)]; A. S. Davydov, in *Biology and Quantum Mechanics* (Pergamon, Oxford, 1982); W. C. Kerr and P. S. Lomdahl, *Phys. Rev. B* **35**, 3629 (1987).
⁹A. C. Scott, *Phys. Rev. A* **26**, 578 (1982); A. C. Scott, *Phys. Scr.* **29**, 279 (1984); L. MacNeil and A. C. Scott, *ibid.* **29**, 284 (1984); A. C. Scott, *Philos. Trans. R. Soc. London, Ser. A* **315**, 423 (1985).
¹⁰P. S. Lomdahl and W. C. Kerr, *Phys. Rev. Lett.* **55**, 1235 (1985); A. F. Lawrence, J. C. McDaniel, D. B. Chang, B. M. Pierce, and R. K. Birge, *Phys. Rev. A* **33**, 1188 (1986); H. Bolterauer, in *Structure, Coherence, and Chaos*, Proceedings of the MIDIT Workshop, 1986, (Manchester University Press, Manchester, 1986) H. Motschmann, W. Förner, and J. Ladik, *J. Phys. Condensed Matter* **1**, 5083 (1989).
¹¹D. W. Brown, K. Lindenberg, and B. J. West, *Phys. Rev. A* **33**, 4104, 4110 (1986); D. W. Brown, *ibid.* **37**, 5010 (1988); D. W. Brown, K. Lindenberg, and B. J. West, *Phys. Rev. B* **35**, 6169 (1987); **37**, 2946 (1988); B. Mechtly and P. B. Shaw, *ibid.* **38**, 3075 (1988).
¹²J. A. Krumhansl and D. M. Alexander, in *Structure and Dynamics; Nucleic Acids and Proteins*, edited by E. Clementi and R. H. Sarma (Adenine, New York, 1983), p. 61.
¹³E. Boyland, in *Symposium on Carcinogenesis*, in Proceedings of the Israel Academy of Sciences, Jerusalem, 1968, edited by E. D. Bergmann and B. Pullman (Jerusalem Academic Press, Jerusalem, 1969); J. Ladik, S. Suhai, and M. Seel, *Int. J. Quantum Chem. QBS5*, 35 (1978); J. Ladik, *ibid.* **QBS13**, 307 (1986); A. K. Bakhshi, J. Ladik, M. Seel, and P. Otto, *Chem. Phys.* **108**, 223 (1986); K. Laki and J. Ladik, *Int. J. Quantum Chem. QBS3*, 51 (1976); F. Beleznyay, S. Suhai, and J. Ladik *ibid.* **20**, 683 (1981).
¹⁴J. Ladik and J. Čížek, *Int. J. Quantum Chem.* **26**, 955 (1984); J. Ladik, in *Molecular Basis of Cancer, Part A*, edited by R. Rein (A. Liss, New York, 1985), p. 343.
¹⁵D. Hofmann, W. Förner, and J. Ladik, *Phys. Rev. A* **37**, 4429 (1988).
¹⁶W. Förner, *Phys. Rev. A* **38**, 939 (1988).
¹⁷K. S. Pfitzer, *Adv. Chem. Phys.* **2**, 59 (1959).
¹⁸J. Ladik, P. Otto, and W. Förner, *Int. J. Quantum Chem. QBS10*, 73 (1983).
¹⁹W. Förner, P. Otto, and J. Ladik, *Chem. Phys.* **86**, 49 (1984).
²⁰P. Otto, *Int. J. Quantum Chem.* **28**, 895 (1985).
²¹P. Otto, *Int. J. Quantum Chem.* **30**, 275 (1986).
²²P. Otto, *J. Mol. Struct.* **188**, 277 (1989).
²³P. Saalfrank, P. Otto, and J. Ladik, *Chem. Phys. Lett.* **153**, 451 (1988).
²⁴W. Förner, J. Ladik, P. Otto, and F. Martino, following paper, *Phys. Rev. A* **40**, 6457 (1989).
²⁵M. Aida and C. Nagata, *Chem. Phys. Lett.* **86**, 44 (1982).
²⁶Y. K. Khang and M. Jhon, *Theor. Chim. Acta* **61**, 41 (1982).
²⁷M. Abramowitz and I. A. Stegun, *Handbook of Mathematical Functions* (Dover, New York, 1972), Eq. 25.5.20, p. 897.
²⁸D. Hofmann, W. Förner, and J. Ladik (unpublished).
²⁹J. A. Pople and W. Hehre, *GAUSSIAN 74*, Indiana University

Quantum Chemistry Program Exchange (QCPE) Program No. 236.

³⁰J. Langlet, P. Claverie, F. Caron, and J. Bouive, *Int. J. Quantum Chem.* **19**, 299 (1981).

³¹See, e.g., H. Goldstein, *Klassische Mechanik* (Akademische

Verlagsgesellschaft, Frankfurt am Main, Federal Republic of Germany, 1974), p. 58.

³²D. Hofmann, W. Förner, and J. Ladik, *J. Phys. Condensed Matter* (to be published).